2018

Detection and Discrimination of Natural and Synthetic Polysaccharides in a Solid-State Nanopore

Jonathan Nichols
University of Rhode Island, jnichols1@uri.edu

DETECTION AND DISCRIMINATION OF NATURAL AND SYNTHETIC POLYSACCHARIDES IN A SOLID-STATE NANOPORE

BY

JONATHAN NICHOLS

A THESIS SUBMITTED IN PARTIAL FULFILLMENT OF THE REQUIREMENTS FOR THE DEGREE OF

MASTER OF SCIENCE

IN

CHEMISTRY

UNIVERSITY OF RHODE ISLAND

2018

MASTER OF SCIENCE IN CHEMISTRY THESIS

OF

JONATHAN NICHOLS

APPROVED:

Thesis Committee:

Major Professor Jason R. Dwyer

Jiyeon Kim

Matthew Kiesewetter

Stephen Kennedy

Nasser H. Zawia
DEAN OF THE GRADUATE SCHOOL

UNIVERSITY OF RHODE ISLAND
2018

ABSTRACT

In 2007-08 over 100 people died as a result of a contaminated batch of the polysaccharide heparin, an otherwise life-saving anticoagulant drug. After the contaminant was discovered, the development of assays that detect the contaminant, a structurally similar molecule, oversulfated chondroitin sulfate, became a necessity. Solid-state nanopores, which can, with appropriate experimental design, readily detect single molecules of analyte, may be able to help distinguish the two with greater ease than conventional assays, and with greater throughput even at concentrations well below that of USP assays. Polysaccharides, especially naturally occurring polysaccharides, have a vast range of structures characterized by widely varying molecular weights and charge distributions, and variability in linkage type. These polymers are challenging to analyze, and so studies using synthetic glycopolymers with known sizes and charge distributions, should be able to help one establish conditions to probe differences in molecular structure more easily. Under the right experimental conditions, solid-state nanopores were readily able to detect and distinguish between oversulfated chondroitin sulfate and heparin, and also synthetic glycopolymers of varying charge and length. This work may provide the necessary context to use nanopores for drug purity assays, to aid in understanding glycopolymer interactions, and also as a tool for characterizing polysaccharide structure and properties.

ACKNOWLEDGMENTS

I would first like to thank Dr. Jason Dwyer for all of his help and guidance in and out of the lab since I joined his research group in January 2016. His enthusiasm for science and learning extends far beyond the classroom and I wouldn't be where I am today without him. I will miss hearing about the crazy stories he has from his graduate student and post-doc experiences. I also thank my committee members, Dr. Stephen Kennedy, Dr. Jiyeon Kim, and Dr. Matthew Kiesewetter for their time serving on my committee.

I would also like to thank my other group members, Nuwan, Buddini, Rob, James, Melissa, and Julie for their help in the lab and research ideas that have helped me accomplish this work. I wish the best of luck to Nuwan and Buddini who are also graduating this year. I don't know of a smarter husband and wife combo than them.

I would next like to thank my friends and family members for their support and for providing me motivation to attend graduate school and follow my dreams. My Mom, being a three time leukemia survivor, for providing me with the strength and determination to pursue my career goals. My girlfriend Kyla, I am extremely excited to finally graduate and start my life with you. You started your career years ago, and it's finally time for me to start mine, too. Thanks for putting up with me for so long, I know I can be a handful at times. After graduation, let's go to the Cod and Venus to get a buffalo chicken pizza and a beer together. I'm sure our Nanas will be happy seeing us at graduation from above, may they both rest in peace.

PREFACE

This thesis has been completed in manuscript format, and completed with two separate manuscripts.

Naturally occurring glycans are inarguably one of the most important classes of biologically active molecules, yet due to their complex chemical properties they are weakly characterized. Their roles extend across a multitude of biological processes[1-10], but most recently the safety of therapeutic glycans has come into question[11]. Heparin, a linear unbranched glycan of the glycosaminoglycan family extracted from porcine intestinal mucosa, is a highly sulfated glycan with the largest negative charge density of any biologically active molecule and is a life-saving anticoagulant drug. However, in 2007-08 the deliberate adulteration of heparin resulted in mortality and morbidity across the world, resulting in widespread panic about the safety of this drug. The contaminant responsible for the observed adverse reactions was identified as oversulfated chondroitin sulfate[12], a more sulfated version of the osteoarthritis supplement chondroitin sulfate, which bears an extremely similar structure to heparin. As a result of the contamination crisis, methods for distinguishing between the two molecules became a necessity. Possible synthetic alternatives to heparin, glycopolymers, have also been considered[13].

In the first manuscript of this thesis, nanopores, which have the ability to detect single molecules at a time, were used to distinguish heparin from oversulfated chondroitin sulfate. Preliminary results showed that resistive pulse nanopore measurements are able to distinguish between the two molecules, and after careful

optimization nanopores may serve as useful mediums in drug purity screening devices in the future. Different samples of the glycan sodium alginate were also analyzed with resistive pulse nanopore measurements and were able to highlight the differences in molecular structure of the two samples.

In the second manuscript, nanopores were used to detect synthetic glycopolymers generated by ring opening metathesis polymerization, from the group of Amit Basu at Brown University[14]. Glycopolymers have been shown to serve as natural glycan analogs and unlike natural glycans, have well characterized properties. This has allowed systematic studies of glycopolymer structure versus biological activity to be established elsewhere. Here we show that under the right experimental conditions, glycopolymers of differing length and charge can be selectively detected and differentiated in resistive pulse nanopore measurements, and they can also probe interactions of glycopolymers with other species. This work has highlighted the potential to study glycopolymer interactions at the single molecule level.

TABLE OF CONTENTS

LIST OF TABLES

LIST OF FIGURES

Tasty, Therapeutic, or Toxic? Gauging Thin-Film Solid-State Nanopores for Polysaccharide Sensing

Buddini Iroshika Karawdeniya, Y.M. Nuwan D.Y. Bandara, Jonathan W. Nichols, Robert B. Chevalier, and Jason R. Dwyer*

Department of Chemistry, University of Rhode Island, 140 Flagg Road, Kingston, 02881, USA.

*jason_dwyer@uri.edu

This manuscript has been submitted to the journal Nature Communications and is currently under revision.

ABSTRACT: Polysaccharides have key roles in a multitude of biological functions, and they can be harnessed for therapeutic roles, with the clinically ubiquitous anticoagulant heparin being a standout example. Their complexity—*e.g*. >100 naturally occurring monosaccharides with variety in linkage and branching structure—significantly complicates their analysis in comparison to other biopolymers such as DNA and proteins. More, and improved, analysis tools have been called for, and we demonstrate that solid-state silicon nitride nanopore sensors and tuned sensing conditions can be used to reliably detect native polysaccharides and enzymatic digestion products, to differentiate between different polysaccharides in straightforward assays, to provide new experimental insights into nanopore electrokinetics, and to uncover polysaccharide properties. Nanopore sensing allowed us to easily differentiate between a clinical heparin sample and one spiked with the contaminant that caused deaths in 2008 when its presence went undetected by conventional assays. The work reported here lays the foundation to further explore polysaccharide characterization and develop assays using thin-film solid-state nanopore sensors.

Oligo- and polysaccharides are ubiquitous in nature, with a broad spectrum of roles that includes energy-storage and provision (including as a foodstuff), structural building block (e.g. cellulose), therapeutic function (e.g. the anticoagulant heparin), and a vital part in biological recognition processes.[1-11] Conventional chemical analysis tools are frequently challenged by the daunting complexity of polysaccharide analysis:[12, 13] identification of monomer composition (~120 naturally occurring monomers!) and sequence, monomer linkage types, stereochemistry, polymer length, and degree of polymer branching.[13] These challenges were tragically driven home in 2008 when undetected contamination of the common anticoagulant heparin by a structurally similar adulterant, oversulfated chondroitin sulfate (OSCS), resulted in profoundly adverse clinical consequences in the United States, including ~100 deaths.[14-19].

Glycan samples can be challenged by heterogeneity and low abundance in addition to chemical and structural diversity, so while new analysis tools have been broadly called for,[12, 13, 20] single-molecule-sensitive methods are a particularly compelling goal for glycomics—more so given the absence of sample amplification techniques analogous to PCR for DNA sequencing[21]. Nanopore single-molecule methods have emerged as a powerful tool for characterizing DNA and proteins including aspects of sequence, structure, and interactions.[22-28] Monomer-resolved length determinations of more prosaic polyethylene glycol samples further buttress the potential of suitably configured nanopore assays for the analysis of polymers with biological utility.[29] The simplest implementation for nanopore measurements places the nanopore—a <100 nm-long nanofluidic channel through an insulating membrane—between two electrolyte solutions (Figure 1). Ion passage through the nanopore in response to a voltage applied across the pore gives the baseline "open pore" current, i_0; passage of a molecule into, across, or through the nanopore disrupts this ion flow to give a blocked-pore current, i_b. A discernible current perturbation reveals the presence of an analyte, and the sign, magnitude, and temporal structure of i_b depend strongly on size and shape of the analyte—and of the nanopore—and on the applied voltage and bulk and interfacial charge distributions. It thus provides insight into analyte presence, identity, and properties, including interactions between the analyte and pore interior or surface.[29-32] Analysis of the resistive-pulse characteristics of a sample offers the potential to glean molecular-level insights, but the i_b characteristics can also be used more simply as benchmarks in quality assurance assays where atypical i_b signal sample impurities.

Much groundwork must be laid, including proof-of-principle experiments, if nanopore methods are to emerge as a tool for glycan profiling—and by extension as a tool for –omics writ-large (spanning genomics, proteomics, and glycomics). Protein nanopores, polymer, and glass-supported nanopores have been used to detect sugar-pore binding, polysaccharides, and

enzyme-digested oligosaccharides.[33-42] While solid-state nanopores in thin (~10 nm) membranes have been often portrayed as the preeminent nanopore platform, their use to profile classes of molecules beyond DNA and proteins is in its infancy. These nanopores can be size-tuned[43] to match analyte dimensions (especially relevant for branched polysaccharides), and when fabricated from conventional nanofabrication materials such as silicon nitride (SiN_x),[44, 45] offer resistance to chemical and mechanical insult alongside low barriers to large-scale manufacturing and device integration. The potential for integration of additional instrumentation components, such as control and readout electrodes, around the thin-film nanopore core, is especially compelling.[28, 44, 45] Recent (nanopore-free) work on recognition electron tunneling measurements on polysaccharides, for example, has reaffirmed the importance of a nanopore development path that values augmented nanopore sensing capabilities.[46] A key question concerning the use of SiN_x nanopores for polysaccharide sensing is whether this fabrication material is compatible with sensing glycans. The often challenging surface chemistry of SiN_x (giving rise to a complex surface charge distribution)[44, 45, 47] may lead to analyte-pore interactions that hinder or prevent its use. Variability in polysaccharide electrokinetic mobility arising from differences in molecular structures may exacerbate the effect of these interactions. These issues become particularly important when analyte translocation through a constricted pore is required, such as in transverse electron tunneling measurements.[28, 46]

The aims of the present work were threefold: (1) to introduce and test the feasibility of SiN_x nanopores for sensing polysaccharides; (2) to explore the preliminary performance of this class of nanopores in this implementation; and (3) to gauge the prospects of a clinically relevant assay to detect a toxic impurity in the anticoagulant heparin. The broader implications of the successful use of SiN_x—a readily nanofabrication-compatible material—to form the nanopores would be to conceivably smooth the path to large-scale production and to provide a

platform amenable to modification for nanopore sensing configurations beyond resistive pulse sensing. We chose a set of polysaccharides with varied compositions to both gauge performance and challenge the SiN_x nanopores. Naturally occurring sodium alginate, with applications in biomedical and food industries, presents an overall negative, but unexceptional, formal charge in neutral pH aqueous solutions. We used samples from two different suppliers—*A1* (Alfa Aesar; M_n~74 kDa based on viscosity measurements) and *A2* (FMC Corporation; M_n~18 kDa based on viscosity measurements)—to explore the sourcing variability for a sample extracted from seaweed.[48] This variability can be as prosaic as molecular weight to more enticing changes in the relative abundances of alginate's constituent mannuronate (M) and guluronate (G) residues.[48] In contrast to alginate, heparin, the prevalent anticoagulant drug, is the most highly negative charge-dense biological molecule known.[49] This exceptional charge density couples with the demonstrated difficulty, by other methods, of detecting the negatively charged oversulfated chondroitin sulfate (OSCS; contaminant molecular weight ~17 kDa[50]) in a heparin sample[14-17] to make the analysis of heparin (~16 kDa) and OSCS by nanopore a compelling experimental test with clinical relevance.

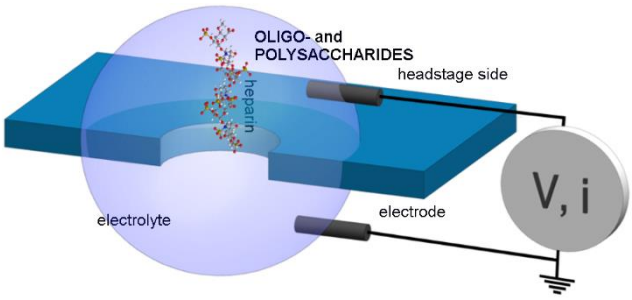

Figure 1 : Schematic of the nanopore setup. Analyte was added to the headstage side ("cis-" side, according to nanopore convention) unless otherwise noted, and applied voltages were referenced to the ground electrode ("trans-" side) on the other side.

RESULTS

Introduction of anionic alginate *A1* (M_n~74 kDa) into the headstage sample well failed to generate detectable transient current changes when a negative headstage voltage (the polarity consistent with purely electrophoretic motion for an anionic analyte) was applied with the analyte in the same well (Figure 1). Application of a positive potential, instead, generated transient current changes (here denoted "events") that could be readily differentiated from the open current noise with ~60:1 event-to-noise frequency compared to analyte-free scans. Figure 2 shows a representative time trace of *A1*-induced events, with a characteristic event magnified. The frequency of discrete current blockages associated with the addition of *A1* showed a linear increase with analyte concentration (Supplementary Figure 1), so that regardless of mechanism, with appropriate measurement conditions, the event frequency can be used to determine the analyte concentration. The mechanism of *A1*-induced signal generation was investigated in a series of experiments. Using a setup (Supplementary Figure 2) that physically separated electrodes and nanopore, events were only detected when *A1* was

injected into the well proximal to the nanopore, thus supporting a signal generation mechanism involving interaction with the nanopore and not with the electrodes. This result did not, however, distinguish between passage-free collision with the nanopore opening ("bumping" or "blocking") or translocation through the pore.[32] Either mechanism (including extending the idea of "bumping" or "blocking" to allow for transient interactions of the analyte with the pore mouth), though, has the potential to deliver analytically useful sensing performance. Low analyte concentrations challenge the direct investigation of polysaccharide translocation through small, single nanopores. In one experiment to investigate this, a solution of *A1* was added to the headstage side of a ~22 nm-diameter nanopore and was left overnight with a +200 mV applied voltage. The initially analyte-free contents of the ground-stage side were then transferred to the headstage side of a fresh ~17 nm-diameter pore, and an appreciable number of *A1*-characteristic events (182 in 1 h) were detected again at +200 mV. Acid digestion was used as a signal generation and amplification technique (complete details in the Supplementary Information) to convert *A1* polymers to many smaller fragment-derived species absorbing at ~270 nm.[51, 52] This spectrophotometric assay (Supplementary Figure 3) was used to confirm translocation of polysaccharide through a ~9 nm SiN_x nanopore.

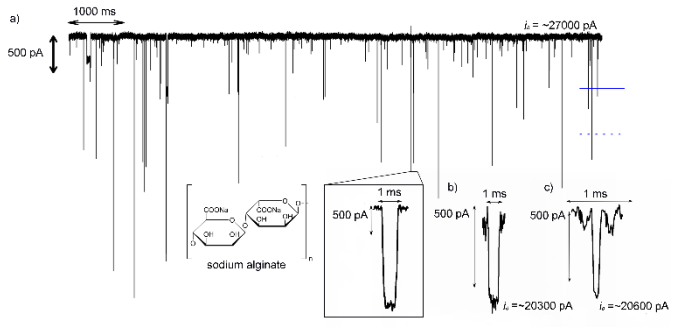

Figure 2. Representative nanopore current trace and events from sodium alginate samples from two different sources. a) A representative segment of an *A1*-induced current trace using a ~22 nm-diameter pore; the solid blue line marks the most frequent event level, $\langle i_b \rangle$, and the blue dashed line is its mean across all events. The magnified current event is from the same trace. b) *A2*- and c) enzyme-digested-*A2*-associated single events through a ~22 nm-diameter pore. All currents were measured in response to a 200 mV applied voltage.

The analyte-induced translocation blockage current, i_b, is expected to be determined by the properties of the analyte and its size relative to the nanopore, among other experimental factors (including interfacial phenomena).[30, 32] For each individual current blockage, we calculated the blockage duration, τ, and the fractional blockage current magnitude, $f_b = \langle i_b \rangle / \langle i_0 \rangle$,where $\langle \ldots \rangle$ denotes a time-average, and i_0 is the current through the pore when unobstructed by analyte. Plots of number of events as a function of τ and f_b (Figure 3) provide an overarching summary of the total current trace. Given detectable differences as a function of analyte, such plots and other representations have the potential to function as analyte fingerprints in quality assurance assays. Fingerprints for *A1* are shown in Figure 3,

acquired in 1 M KCl, pH ~7 solutions using a +200 mV applied voltage. Supplementary Figures 4 and 5 provide alternative presentations of the experimental measurements. The (most frequent) f_b increased in magnitude with increasing nanopore radius, r_{pore} (that is, the relative magnitude of the current perturbations due to the analyte were reduced). This parallels the behaviour observed in studies of DNA translocation that could be described using a simple volume-exclusion framework: $r^2_{analyte}/r^2_{pore} = 1 - f_b$. While nanopore diameters are fixed once fabricated (absent etching), a conformationally flexible macromolecule can present a range of apparent cross-sections to a nanopore, down to its molecular cross-section if linearized by a sufficiently small nanopore. In such a case, the nanopore geometric constraints can increase the end-to-end length of the translocating nanopore or, depending on the nature of the analyte, expose surface chemistry that can similarly affect translocation times. In Figure 3d, the use of a ~5 nm-diameter nanopore broadened the distribution of f_b and produced deeper blockages with longer durations than when using the larger nanopore. Lowering the electrolyte concentration can have a dramatic effect on nanopore sensing, through changes in the bulk and at interfaces. For example, reducing the ion concentration from 1 to 0.1 M KCl increases the Debye layer thickness changing the electrostatic size of the pore with consequences for electrokinetic phenomena, and electroosmosis especially. Comparing Figures 3a and 3e, this change of concentration did not affect the voltage polarity needed to generate events, but decreased the f_b for the same experimental configuration, and appreciably lengthened the (most frequent) blockage duration. More profoundly, the 10-fold salt concentration decrease reduced the frequency of events 6-fold in the same size ~18 nm-diameter pore. We found, and exploited in a more general context for the sensing of heparin and OSCS (below), that such a simple change of electrolyte concentration is a powerful parameter for tuning our ability to sense polysaccharides. Changing the electrolyte pH offers a similar parameter for tuning the sensing performance of nanopores with ionizable surface groups. The surface charge of SiN_x nanopores can be tuned from negative through its isoelectric point (~4.3±0.3) to positive,[44, 53]

and the consequence of this pH change is seen in Supplementary Figure 6: the voltage polarity for signal generation is opposite at pH 3 and 5 (and opposite to the electrophoretic direction for all pH values), and the event frequency is at its minimum nearest the isoelectric point and increases with increase and decrease in pH from this point.

After the initial exploratory and proof-of-principle experiments using *A1*, we turned to the second sodium alginate sample, *A2*, obtained from a separate supplier. In general, the interplay between analyte charge density, monomer chemical nature and polymer linkages, and electrolyte composition, is expected to influence nanopore sensing. Experiments showing the polarity-dependence of event occurrence, and its frequency, as a function of pH showed the same qualitative behaviour as for *A1* in Supplementary Figure 6, but with lower event frequencies overall. Both alginate samples were readily digested by alginate lyase (Supplementary Figure 3),[54] but infrared spectroscopy showed that *A2* contained a dramatically greater proportion of carboxylate groups than *A1* (Supplementary Figure 7), so that the overall charge density of this molecule was expected to be higher than *A1*. Further analysis was consistent with alginate *A1* having a ratio of guluoronic (G) to mannuronic (M) residues exceeding that of *A2*, with values from IR spectroscopy of ~63%G/37%M and ~57%G/43%M, respectively.[48] Nanopore profiling of *A2* showed differences compared to *A1*. Using the same electrolyte for *A2* as for *A1*, measurements generated a ~7-fold lower event frequency with longer durations for *A2* compared to *A1*, in spite of at the 75-fold higher *A2* concentrations required for reasonable measurement times. Enzymatic digestion of *A2* produced events at a higher frequency than for undigested *A2*, but still at lower frequency than for *A1*. The events for the digested sample of *A2* were ten-fold shorter-lived than for the *A2* polymer, but not appreciably different in terms of blockage depth (Figure 3).

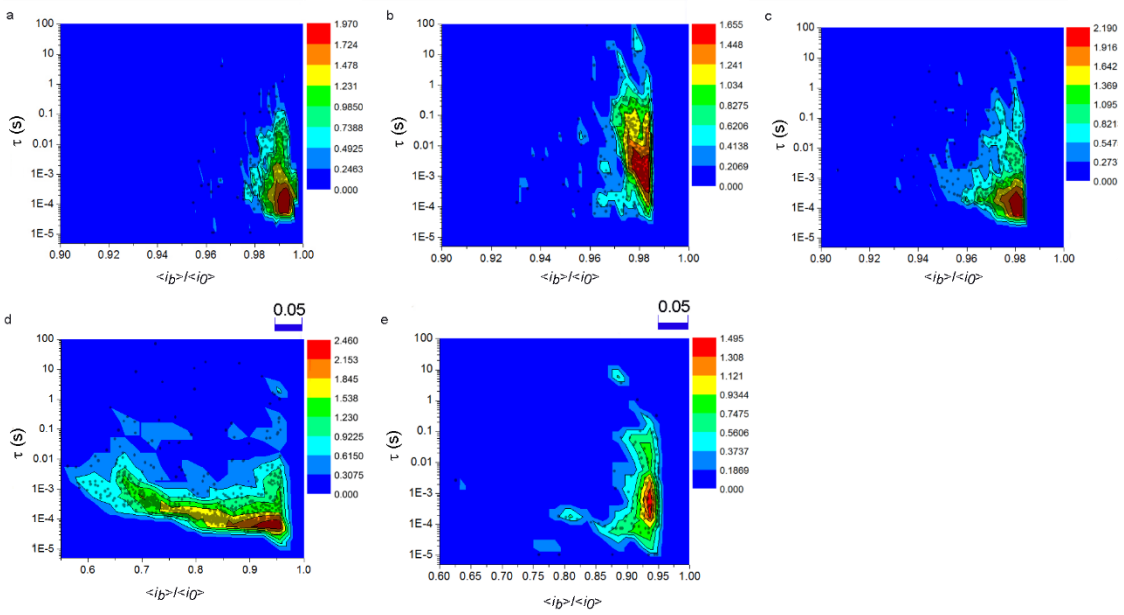

Figure 3: Combination heat map-scatter plots of alginate-induced events. Event counts (plotted as $\log_{10}$ on the colour axis) of a) 4 µL 0.2% (w/v) *A1* using a ~19 nm diameter pore (~0.321 events/s), b) 20 µL of 3% (w/v) *A2* using a ~22 nm (~0.046 events/s) and c) 20 µL of 10-minute enzyme digested 3% (w/v) *A2* using a ~23 nm diameter pore (~0.112 events/s), all in pH ~7 buffered 1 M KCl. The experiment in (a) was repeated d) using a ~5 nm nanopore (~0.403 events/s), and e) an ~18 nm-diameter pore, but in 0.1 M KCl (vs. 1M KCl in (a)) electrolyte buffered at pH ~7 (~0.0527 events/s).

These initial survey experiments showed measurement outcomes with strong sensitivity to analyte identity, with the number of anionic carboxylate moieties being a compelling differentiator between *A1* and *A2*. We then turned to the pressing specific challenge of (anionic) heparin sensing and (anionic) OSCS impurity detection. The first change, from the earlier work, was that the signal generation voltage polarity now corresponded with the conventional electrophoretic direction for an anionic species. Acid digestion experiments akin to those in Supplementary Figure 3 confirmed that heparin could

translocate through the pore in response to an applied voltage. As with *A1*, heparin could be detected in 1 M KCl electrolyte, but the heparin event blockage magnitude and event frequency were both greater in 4 M KCl, and so measurements were performed at this higher salt concentration (see Supplementary Figure 8 for representative events and a heat map). Plots of event frequency versus heparin concentration were linear (Figure 4), with a limit of detection of 0.379 USP heparin units/mL (in a 500 μL well). In comparison, clinical dosage levels of ~10^4 units/day using ~10^3 units/mL stock solutions are not uncommon. Heparin and alginate fingerprints differed in appearance from each other, but also through the profoundly different measurement configuration—opposite applied voltage polarity and fourfold higher electrolyte concentration for heparin—used to acquire them. We were more keenly interested, though, in whether an OSCS impurity in heparin could be detected. We performed measurements on unadulterated USP samples of either heparin or OSCS under identical experimental conditions. On the level of individual events, heparin and OSCS differed in their apparent interaction with the nanopore, with OSCS having a greater propensity to permanently block the pore unless a ~1.3 V ("zap") pulse—a common approach leveraging the electrokinetic basis of analyte motion—was quickly applied when indications suggesting an impending permanent blockage arose. In addition, events associated with the heparin and OSCS samples differed appreciably in the current fluctuations during individual current blockages: OSCS current blockages exhibited ~2–3× greater current noise, $\sigma(f_b)$, than heparin-induced events. Overall, in spite of considerable overlap in the most frequent event f_b and τ, the distribution of event characteristics revealed a key difference between heparin and OSCS samples (Figure 5 and Supplementary Figure 9). Namely, events measured using heparin samples exhibited a longer duration tail in the total event duration distribution, while events measured using OSCS samples exhibited a longer tail in f_b. Measurements of mixtures of heparin and OSCS (16 ppm each) yielded event distributions showing both tails, consistent with the presence of both the heparin therapeutic and its contaminant. We developed an

automatic thresholding procedure based on event distribution statistics in f_b and τ (details in the Supplementary Information) to collapse the event distribution fingerprints into recognition flags denoting the presence or absence of each component. In brief, OSCS was declared present when events occurred with, $f_{b,\,sample} \geq$ mode $(f_{b,}{}^{binned}{}_{USP\ heparin})$-3σ$(f_{b,}{}^{binned}{}_{USP\ heparin})$ and heparin was declared present when events occurred with $\tau_{sample} \geq$ mode $((\log_{10}\tau_{USP\ OSCS})^{binned})$-3σ$((\log_{10}\tau_{USP\ OSCS})^{binned})$. Figure 5 shows the correct recognition of USP heparin, USP OSCS, and a mixture of both, across four trials using nanopores of slightly different sizes. The OSCS contaminant levels detected here were fourfold lower (without efforts to explore a lower bound) than the OSCS detection limit reported in the work that examined and quantified the contaminant in suspect heparin lots.[18]

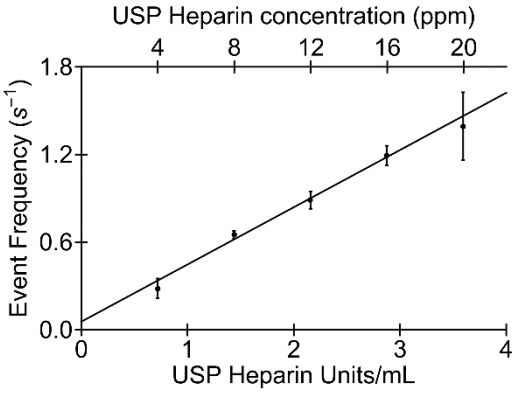

Figure 4: Heparin calibration curve. Three trials were performed, with at least 500 events per run extracted from 900 s-long measurements in a ~9 nm pore at -200 mV applied voltage after consecutive addition of 1 µL aliquots to the head-stage side of the same nanopore. Error bars are the standard deviation for the three trials.

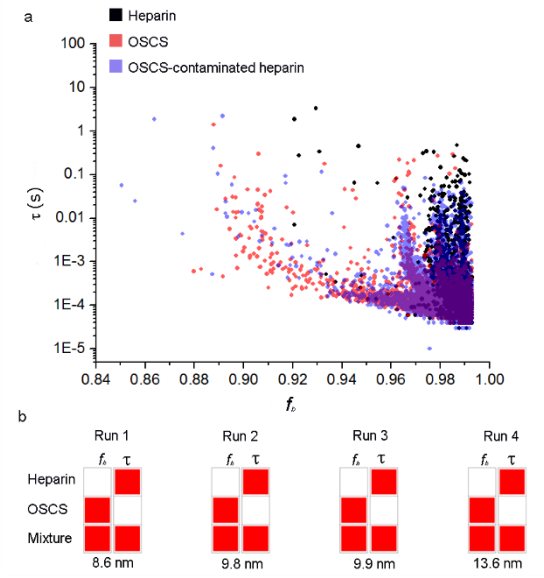

Figure 5: Nanopore resistive-pulse analysis of heparin, OSCS, and their mixture. a) Superimposed scatter plots of 4 µL heparin, OSCS and OSCS-contaminated heparin added to 4 M potassium chloride at -200 mV and measured using a ~14 nm pore. The colours in the legend correspond to the listed sample, and are blended (using transparency) in the plot where events from different samples overlap. b) Recognition flags of heparin, OSCS and their mixture from four independent trials accurately identify the presence of the OSCS aliquot in the mixture.

DISCUSSION

We demonstrated the feasibility of using SiN_x nanopores to characterize glycans exhibiting a variety of chemical compositions, including a prevalent therapeutic, heparin. The extremely high charge density carried by heparin poses a particular challenge to a nanoscale sensor element that can, itself, be charged. More generally, unwanted interactions between analyte and nanopore—and the ease and feasibility of ameliorative steps—can imperil nanopore-based experiments: that none of the diverse polysaccharides considered here catastrophically clogged the nanopore—even when subjected to the stringent test of translocation through the pore–was salutary.[47] Indeed, nanopore sensing was successful over a number of electrolyte concentration ranges, from 0.1 to 4 M KCl, for which shielding of the charged nanopore surface would be quite different in degree. With translocation possible through SiN_x nanopores, even with their charged surface, a rich set of nanopore-based sensing configurations should be within reach. In this work, we used a straightforward resistive-pulse sensing paradigm to readily detect and differentiate between different polysaccharides, including enzymatic digestion products and two separate alginate samples differing in relative monomer composition. We used voltage polarity and electrolyte composition alongside the distribution of events as a function of f_b and τ to construct fingerprints and recognition flags characteristic of each sample. Linear calibration curves show that these measurements easily support concentration determinations in addition to analyte recognition.

From a fundamental perspective, nanopores can be a powerful tool for exploring molecular, interfacial, and intermolecular phenomena, often arising from only simple changes of experimental conditions. Electrolyte-dependent interfacial interactions—at nanopore and molecule surfaces—are complex, and treatments of widely varying levels of sophistication have emerged from decades of experimental and theoretical studies of the canonical nanopore-DNA system, in particular.[32] For example, changes of electrolyte concentration have been

observed to reverse the sign of the current perturbation in DNA translocations through solid-state nanopores, and to decrease dextran sulfate blockage frequencies while increasing their durations using ~1.3 nm-diameter pores where the Debye length was comparable to the pore dimensions.[42, 55] With the larger pores used here, overlapping Debye layers would not be expected in 0.1 M KCl solutions, leaving three expected principal effects of lowering the electrolyte concentration from 1 M KCl: a lowering of the potential across the pore and thus of the overall electrophoretic force on an analyte near the pore; a reduction in the available number of bulk ions displaced by the analyte volume; and a change in the ion distribution around charged interfaces—the nanopore and analyte surfaces—that influences the nanopore signal through a complex overall mechanism within a given experimental configuration. Blockage magnitudes measured here in the more conventional 1 M KCl would be consistent with, in a simple volume exclusion sense ($r_{analyte}^2/r_{pore}^2 = 1 - f_b$), translocation of linearized polysaccharides. Deeper blockages would be expected from the polysaccharides here with hydrodynamic radii on par with the nanopore diameters. Polysaccharide translocation was independently confirmed and signals were generated only when the analytes had access to the nanopores, so these events either arose from analyte interactions with the pore mouth rather than from complete translocation, or the blockage magnitude analysis must include additional factors such as charge density carried by the analyte, itself, and mobile charge at the analyte-solution and solution-nanopore interfaces.[55, 56] The effects of these and more complex interfacial phenomena emerged in one of the more startling observations in this work: that the voltage polarity for signal generation with both alginate samples was opposite to that expected for electrophoretic motion of an anionic polymer, whereas for heparin the voltage polarity was consistent with electrophoresis. In addition, when comparing the two alginates, the more charge-rich *A2* was detected at a lower event frequency than *A1*. Nanopore–based studies with polyethylene glycol polymers point to a change of effective analyte charge by sorption of electrolyte ions (K^+ for those studies) with the resultant analyte motion then being

electrophoretic for the voltage polarity and the sign of the sorbed charge.[29] The results of Supplementary Figure 6, however, point to pH-dependent changes in the voltage polarity required for sensing alginates, with the polarity having opposite signs on either side of the isoelectric point of SiN_x. Mirroring this change in the voltage polarity is the SiN_x surface charge that is positive at lower pH and negative at higher pH. This change in surface charge sign causes a reversal in the direction of electroosmotic motion for a fixed voltage polarity (and thus fixed electrophoretic direction).[44, 45] The apparent mobility of an analyte in response to electrolyte flow through the surface-charged nanochannel is the sum of its electrophoretic and electroosmotic mobilities. Changes of solution pH can then tune the apparent analyte mobility and even overall direction of analyte motion. Changes of solution pH can also affect the charge density and sign of analytes (and thus the voltage polarity required for electrophoresis in a given direction) containing at least one acidic or basic functional group as determined by the balance of acid-base equilibria (determined by functional group abundance and pK_a). Given the acidic functional groups in the analytes here, the changes in nanopore surface chemistry should dominate the effective mobility and its voltage polarity dependence. The event frequency and voltage polarity behaviours are consistent with the distinct physicochemical properties of each analyte in a signal generation method in which both electrophoresis and electroosmosis occur simultaneously. Alginate *A1* has the lowest charge density, and thus its electrophoretic response is dominated by electroosmosis with the electrophoretic and electroosmotic driving forces being in opposition in the negatively charged SiN_x pores at pH ~7. Alginate *A2* is more negatively charged and so one would anticipate a stronger electrophoretic driving force; the direction of signal generation is still consistent with electroosmosis. The lower event frequency compared to *A1* can be understood as arising from opposing electrophoretic and electroosmotic driving forces, but with the electrophoretic force on *A2* being greater than on *A1*. More detailed exploration of the differences between *A1* and *A2* must also contend with their different molecular weights and their different chain

flexibilities arising from their different M/G ratios. In the case of heparin, the charge density is sufficiently high so that events are detected using a voltage polarity that would drive the anionic polymer towards the nanopore. Experimental investigations including and beyond the ones presented here, exploring the underpinnings of the nanopore-generated signal using (polysaccharide) biopolymers with greater chemical and structural complexity than the canonical nanopore test molecule, DNA, or than homopolymers such as polyethylene glycol, should also provide fertile ground for high-level simulations. Interfacial effects will require additional study in the context of polysaccharides, but hold possibilities for tuning sensing selectivity and sensitivity. Indeed, explicit consideration of sensing conditions—including nanopore size, electrolyte composition, and voltage polarity—already augments the ability to compare nanopore molecular fingerprints as shown in Figure 3.

The failure in 2008 to detect an OSCS contaminant in clinical heparin samples had previously led to patient morbidity and mortality,[14-18] so that our ability to use a simple nanopore-based assay to quantify heparin levels and detect OSCS at clinically meaningful contamination levels, is itself significant. In a broader sense, we expect that these initial results exploring polysaccharide structure can, by analogy with earlier nanopore DNA and protein sensing supporting genomics and proteomics, spotlight the potential of using nanopores as a tool for glycomics. The demonstration of polysaccharide translocation through nanofabrication-compatible SiN_x nanopores portends the development of more sophisticated sensing schemes as seen in the use of nanopores for genomics. Similarly, the successful use of chemical tuning—of electrolyte composition and by enzyme addition—to alter the nanopore signal generated by diverse polysaccharides suggests that nanopore glycomics might borrow from and extend upon similar approaches developed for nanopore genomics. There is an ongoing need in glycomics for new tools to cope with the analytical challenges caused by the structural and physicochemical complexity of polysaccharides, and by the often inherently

heterogenous nature of naturally derived carbohydrates. The demonstrations of nanopore sensing here provide a beachhead for ongoing efforts to develop solid-state nanopores as a promising platform technology for glycomics.

METHODS

A full listing of the experimental details is available in the Supplementary Information. Nanopores were formed via dielectric breakdown[43] in nominally 10 nm-thick silicon nitride (SiN_x) membranes. Nanopore sizes were inferred from their conductance, G, determined from Ohmic current-voltage data. Nanopores used for measurements produced stable open-pore (analyte-free) currents in the electrolyte solutions used. Polysaccharides were commercially obtained: sodium alginate samples from two different sources - *A1* (Alfa Aesar, Ward Hill, MA) and *A2* (FMC Corporation Health and Nutrition, PA, USA); USP heparin sodium salt; and USP OSCS. For routine measurements, sample aliquots were added to the headstage side (Figure 1), leaving the ground side free of initially added analyte. Current blockages were extracted using a current-threshold analysis. All applied voltages are stated with the polarity of the electrode on the headstage side relative to ground on the ground side of the sample cell.

AUTHOR INFORMATION

Corresponding Author

Email: jason_dwyer@uri.edu

Author Contributions

All authors have contributed to, and approve, the manuscript.

Acknowledgements

This research has been supported by NSF CAREER award CBET-1150085, and by the University of Rhode Island, including URI graduate fellowships for Y. M. Nuwan D. Y. Bandara and Buddini Iroshika Karawdeniya. We thank Travis Leffert for preliminary polysaccharide measurements. We thank the Lucht Group (URI Dept. of Chemistry) for access to their IR spectrometer, and K.W.D. Kaveendi Chandrasiri and Bharathy S. Parimalam for acquiring IR spectra. We thank the group of Prof. Stephen Kennedy (URI Depts. Of Electrical, Computer and Biomedical Engineering, & Chemical Engineering) for samples of alginate *A2*.

REFERENCES

1. Imberty, A. & Pérez, S. Structure, Conformation, and Dynamics of Bioactive Oligosaccharides: Theoretical Approaches and Experimental Validations. *Chem. Rev.* **100**, 4567-4588 (2000).
2. DeMarco, M.L. & Woods, R.J. Structural glycobiology: A game of snakes and ladders. *Glycobiology* **18**, 426-440 (2008).
3. Dove, A. The bittersweet promise of glycobiology. *Nature Biotechnology* **19**, 913-917 (2001).
4. Ernst, B. & Magnani, J.L. From carbohydrate leads to glycomimetic drugs. *Nat Rev Drug Discov* **8**, 661-677 (2009).
5. Pinho, S.S. & Reis, C.A. Glycosylation in cancer: mechanisms and clinical implications. *Nat Rev Cancer* **15**, 540-555 (2015).
6. Seeberger, P.H. Chemical glycobiology: why now? *Nat Chem Biol* **5**, 368-372 (2009).
7. Lichtenstein, R.G. & Rabinovich, G.A. Glycobiology of cell death: when glycans and lectins govern cell fate. *Cell Death Differ* **20**, 976-986 (2013).
8. Dalziel, M., Crispin, M., Scanlan, C.N., Zitzmann, N. & Dwek, R.A. Emerging Principles for the Therapeutic Exploitation of Glycosylation. *Science* **343** (2014).
9. Essentials of Glycobiology, Edn. 2. (Cold Spring Harbor Laboratory Press, 2009).
10. Linhardt, R.J. & Toida, T. Role of Glycosaminoglycans in Cellular Communication. *Acc. Chem. Res.* **37**, 431-438 (2004).
11. Kovalenko, I. et al. A Major Constituent of Brown Algae for Use in High-Capacity Li-Ion Batteries. *Science* **334**, 75-79 (2011).
12. National Research Council Transforming Glycoscience: A Roadmap for the Future. (The National Academies Press, Washington, DC; 2012).
13. Czjzek, M. Biochemistry: A wine-induced breakdown. *Nature* **544**, 45-46 (2017).
14. Lester, J., Chandler, T. & Gemene, K.L. Reversible Electrochemical Sensor for Detection of High-Charge Density Polyanion Contaminants in Heparin. *Anal. Chem.* **87**, 11537-11543 (2015).
15. Kim, D.-H., Park, Y.J., Jung, K.H. & Lee, K.-H. Ratiometric Detection of Nanomolar Concentrations of Heparin in Serum and Plasma Samples Using a Fluorescent Chemosensor Based on Peptides. *Anal. Chem.* **86**, 6580-6586 (2014).
16. Liu, H., Zhang, Z. & Linhardt, R.J. Lessons learned from the contamination of heparin. *Natural Product Reports* **26**, 313-321 (2009).

17. Korir, A. & Larive, C. Advances in the separation, sensitive detection, and characterization of heparin and heparan sulfate. *Analytical & Bioanalytical Chemistry* **393**, 155-169 (2009).
18. Kishimoto , T.K. et al. Contaminated Heparin Associated with Adverse Clinical Events and Activation of the Contact System. *New England Journal of Medicine* **358**, 2457-2467 (2008).
19. Guerrini, M. et al. Oversulfated chondroitin sulfate is a contaminant in heparin associated with adverse clinical events. *Nat Biotech* **26**, 669-675 (2008).
20. Kailemia, M.J., Ruhaak, L.R., Lebrilla, C.B. & Amster, I.J. Oligosaccharide Analysis by Mass Spectrometry: A Review of Recent Developments. *Anal. Chem.* **86**, 196-212 (2014).
21. Kasianowicz, J.J., Brandin, E., Branton, D. & Deamer, D.W. Characterization of individual polynucleotide molecules using a membrane channel. *Proceedings of the National Academy of Sciences* **93**, 13770-13773 (1996).
22. Haywood, D.G., Saha-Shah, A., Baker, L.A. & Jacobson, S.C. Fundamental Studies of Nanofluidics: Nanopores, Nanochannels, and Nanopipets. *Anal. Chem.* **87**, 172-187 (2015).
23. Taniguchi, M. Selective Multidetection Using Nanopores. *Anal. Chem.* **87**, 188-199 (2015).
24. Reiner, J.E. et al. Disease Detection and Management via Single Nanopore-Based Sensors. *Chem. Rev.* **112**, 6431-6451 (2012).
25. Howorka, S. & Siwy, Z. Nanopore analytics: sensing of single molecules. *Chem. Soc. Rev.* **38**, 2360-2384 (2009).
26. Miles, B.N. et al. Single Molecule Sensing with Solid-State Nanopores: Novel Materials, Methods, and Applications. *Chem. Soc. Rev.* **42**, 15-28 (2013).
27. Oukhaled, A., Bacri, L., Pastoriza-Gallego, M., Betton, J.-M. & Pelta, J. Sensing Proteins through Nanopores: Fundamental to Applications. *ACS Chemical Biology* **7**, 1935-1949 (2012).
28. Branton, D. et al. The potential and challenges of nanopore sequencing. *Nat. Biotechnol.* **26**, 1146-1153 (2008).
29. Reiner, J.E., Kasianowicz, J.J., Nablo, B.J. & Robertson, J.W.F. Theory for polymer analysis using nanopore-based single-molecule mass spectrometry. *Proceedings of the National Academy of Sciences* **107**, 12080-12085 (2010).
30. Wanunu, M., Sutin, J., McNally, B., Chow, A. & Meller, A. DNA Translocation Governed by Interactions with Solid-State Nanopores. *Biophys. J.* **95**, 4716-4725 (2008).
31. Carbonaro, A. & Sohn, L.L. A resistive-pulse sensor chip for multianalyte immunoassays. *Lab on a Chip* **5** (2005).
32. Aksimentiev, A. Deciphering ionic current signatures of DNA transport through a nanopore. *Nanoscale* **2**, 468-483 (2010).
33. Bacri, L. et al. Discrimination of neutral oligosaccharides through a nanopore. *Biochem. Biophys. Res. Commun.* **412**, 561-564 (2011).
34. Fennouri, A. et al. Single Molecule Detection of Glycosaminoglycan Hyaluronic Acid Oligosaccharides and Depolymerization Enzyme Activity Using a Protein Nanopore. *ACS Nano* **6**, 9672-9678 (2012).
35. Fennouri, A. et al. Kinetics of Enzymatic Degradation of High Molecular Weight Polysaccharides through a Nanopore: Experiments and Data-Modeling. *Anal. Chem.* **85**, 8488-8492 (2013).
36. Kullman, L., Winterhalter, M. & Bezrukov, S.M. Transport of Maltodextrins through Maltoporin: A Single-Channel Study. *Biophys. J.* **82**, 803-812 (2002).

37. Zhao, S. et al. Sugar-stimulated robust nanodevice: 4-Carboxyphenylboronic acid modified single glass conical nanopores. *Electrochem. Commun.* **36**, 71-74 (2013).
38. Zheng, Y.-B. et al. A temperature, pH and sugar triple-stimuli-responsive nanofluidic diode. *Nanoscale* **9**, 433-439 (2017).
39. Nguyen, Q.H., Ali, M., Neumann, R. & Ensinger, W. Saccharide/glycoprotein recognition inside synthetic ion channels modified with boronic acid. *Sensors and Actuators B: Chemical* **162**, 216-222 (2012).
40. Vilozny, B. et al. Carbohydrate-actuated nanofluidic diode: switchable current rectification in a nanopipette. *Nanoscale* **5**, 9214-9221 (2013).
41. Sun, Z. et al. pH gated glucose responsive biomimetic single nanochannels. *Chem. Commun.* **48**, 3282-3284 (2012).
42. Oukhaled, G., Bacri, L., Mathé, J., Pelta, J. & Auvray, L. Effect of screening on the transport of polyelectrolytes through nanopores. *EPL (Europhysics Letters)* **82**, 48003 (2008).
43. Kwok, H., Briggs, K. & Tabard-Cossa, V. Nanopore Fabrication by Controlled Dielectric Breakdown. *PLoS ONE* **9**, e92880 (2014).
44. Dwyer, J.R., Bandara, Y.M.N.D.Y., Whelan, J.C., Karawdeniya, B.I. & Nichols, J.W. in Nanofluidics, 2nd Edition, Edn. 2. (eds. J. Edel, A. Ivanov & M. Kim) (Royal Society for Chemistry, 2016).
45. Dwyer, J.R. & Harb, M. Through a Window, Brightly: A Review of Selected Nanofabricated Thin-Film Platforms for Spectroscopy, Imaging, and Detection. *Appl. Spectrosc.* **71**, 2051-2075 (2017).
46. Im, J. et al. Electronic single-molecule identification of carbohydrate isomers by recognition tunnelling. *Nature Communications* **7**, 13868 (2016).
47. Yusko, E.C. et al. Controlling protein translocation through nanopores with bio-inspired fluid walls. *Nature Nanotechnology* **6**, 253-260 (2011).
48. Pereira, L., Sousa, A., Coelho, H., Amado, A.M. & Ribeiro-Claro, P.J.A. Use of FTIR, FT-Raman and 13C-NMR spectroscopy for identification of some seaweed phycocolloids. *Biomol. Eng* **20**, 223-228 (2003).
49. Linhardt, R.J. 2003 Claude S. Hudson Award Address in Carbohydrate Chemistry. Heparin: Structure and Activity. *J. Med. Chem.* **46**, 2551-2564 (2003).
50. Viskov, C. et al. Isolation and Characterization of Contaminants in Recalled Unfractionated Heparin and Low-Molecular-Weight Heparin. *Clinical and Applied Thrombosis/Hemostasis* **15**, 395-401 (2009).
51. Foulger, J.H. THE USE OF THE MOLISCH (α-NAPHTHOL) REACTIONS IN THE STUDY OF SUGARS IN BIOLOGICAL FLUIDS. *J. Biol. Chem* **92**, 345-353 (1931).
52. Hallal, J.L.J., Lucho, A.M.S. & Gonçalves, R.S. Electrochemical polymerization of furfural on a platinum electrode in aqueous solutions of potassium biphthalate. *Materials Research* **8**, 23-29 (2005).
53. Hoogerheide, D.P., Garaj, S. & Golovchenko, J.A. Probing Surface Charge Fluctuations with Solid-State Nanopores. *Phys. Rev. Lett.* **102**, 256804 (2009).
54. Skidmore, M.A., Guimond, S.E., Dumax-Vorzet, A.F., Yates, E.A. & Turnbull, J.E. Disaccharide compositional analysis of heparan sulfate and heparin polysaccharides using UV or high-sensitivity fluorescence (BODIPY) detection. *Nat. Protocols* **5**, 1983-1992 (2010).
55. Smeets, R.M.M. et al. Salt Dependence of Ion Transport and DNA Translocation through Solid-State Nanopores. *Nano Lett.* **6**, 89-95 (2006).
56. Binquan, L. & Aleksei, A. Control and reversal of the electrophoretic force on DNA in a charged nanopore. *J. Phys.: Condens. Matter* **22**, 454123 (2010).

Chapter 2

“Detection and discrimination of glycopolymers in a solid-state nanopore”

Jonathan W. Nichols, Melissa Morris, Y.M. Nuwan D.Y. Bandara, Buddini Iroshika Karawdeniya, Robert B. Chevalier and Jason R. Dwyer*

Department of Chemistry, University of Rhode Island, 140 Flagg Road, Kingston, 02881, USA.

*jason_dwyer@uri.edu

This manuscript is being prepared for submission to the journal Nature Biotechnology.

ABSTRACT: Naturally occurring glycans participate in many of the most biologically relevant chemical reactions known, but their underlying mechanisms are difficult to study due to the complexity of their chemical properties, making the link between chemical structure and observed biological activity very difficult to study. Analysis of glycans by typical chemical analysis methods comes with its own complications, but recent work with solid-state silicon nitride nanopores has shown that glycans can be reliably detected and differentiated, even when chemical structures are similar. Glycopolymers, synthetic polymers with pendant carbohydrate chains and well-known chemical properties, have been shown to serve as useful glycan analogs to study the mechanisms of biological processes. Here we show that a solid-state silicon nitride nanopore can selectively detect and differentiate between glycopolymers of different size and charge, and can be used to probe molecular interactions with another species under the right experimental conditions.

Glycans participate in a wide range of biological functions, such as cellular communication, cell-cell recognition, signal transduction, protein-carbohydrate recognition[1-7], energy storage[8], and therapeutics[9,10]. Perhaps one of the more clinically important polysaccharides is heparin, the most negatively charge dense biomolecule known. It is a life-saving anticoagulant drug derived from porcine intestinal mucosa, which is listed on the 20th WHO model list of essential medicines[11]. However, between 2007 and 2008 over half of the world's heparin supply was recalled due to the deliberate adulteration of heparin products for apparent profit gain[12]. This incident caused widespread panic about the safety of using this essential glycan and resulted in ~100 deaths and increased morbidity among heparin users. Immediate action was taken and the adulterant was determined to be oversulfated chondroitin sulfate (OSCS),

an oversulfated version of the common osteoarthritis supplement chondroitin sulfate[13]. This adulterant went undetected by any United States Pharmacopeia (USP) purity assay at the time, which motivated the search for new methods to distinguish between the two extremely similar molecules. Most recently, nanopores have emerged as a potential purity assay for detecting this impurity[14], but optimization of this process is still undergoing.

Solid-state nanopores have shown great promise as single molecule detectors in DNA sequencing and proteins[15-21]. However, natural glycans exhibit a wide range of structural diversity, such as structure, molecular weight, and branching, which can significantly complicate the analysis of such molecules by common analytical methods. Samples of the same glycan from different manufacturers can have different properties, even color, making analysis of each individual glycan sample necessary, time consuming, and often difficult. If we wish to understand the roles of glycans in biological processes, systematic study of their functions as a function of their molecular structures is required, which in turn requires molecular structure to be known in great detail. Some subclasses of glycopolymers contain pendant carbohydrate groups, and those of synthetic origin are useful glycan analogs because their chemical structure and properties can be known and modified with ease, allowing their biological activity to be linked directly to their molecular properties. Glycopolymers may also serve as safe glycan analogs in therapeutic treatments[22]. The chain length, molecular weight, and charge density of glycopolymers can tuned to one's desired properties with simple changes in synthesis design, using a variety of synthesis methods including atom transfer radical polymerization, reversible addition-fragmentation chain-transfer polymerization and ring opening metathesis polymerization[23-25]. They differ from naturally occurring glycans in their chemical structure. For example, glycosaminoglycans are made of a repeating disaccharide unit. However, glycopolymers can be synthesized to have long hydrophobic

chains with pendant carbohydrate groups off of them. These pendant carbohydrate groups can have substituted hydroxyl groups, for example a sulfate, rendering the group hydrophilic and thus glycopolymers have the ability to form micelles as well.

Glycopolymers have been used as glycosaminoglycan mimics in an array of studies on axon regrowth where glycopolymers were used to mimic chondroitin sulfate proteoglycans[26]. Because the use of these glycopolymers afforded the ability of synthesis of glycopolymers with different chain lengths, links between glycopolymer length and the desired activity were able to be established. On top of being a useful analog to study many types of interactions, we hypothesize that glycopolymers may also serve as a great glycan analog in nanopore measurements and allow glycan activity to be studied at the single molecule level.

Nanopores are channels through an insulating membrane less than 100 nm in all directions surrounded by electrolyte on both sides and can be classified as natural or solid state. Passage of glycans has been reported in natural α-hemolysin and aerolysin pores[27-30], and also solid-state glass[31] and most recently silicon nitride (SiN_x) nanopores[14]. Due to their robustness and ease of formation, solid-state SiN_x nanopores were used in this study. Application of a voltage across the nanopore by placing electrodes in both electrolyte solutions, which surround the nanopore, produces an open pore current, I_0. When passage of a molecule through the nanopore occurs, the current flowing through the nanopore is perturbed, and a blockage current, I, is recorded. Analysis of the magnitude, duration, and shape characteristics of I gives insight into the hydrodynamic diameter of the molecule, its orientation, and possible interactions with the nanopore surface. Details of the experimental configuration needed to obtain current blockages provides details of the analyte charge (if not

known) depending on the electrophoretic and/or electroosmotic flow of analyte movement through the nanopore. Nanopore dimensions can be tuned to one's needs with simple experimental preparation procedures to ensure that the dimensions of the nanopore are consistent with that of the analyte. Experimental configuration parameters such as electrolyte concentration, pH, and applied voltage across the nanopore can be optimized to ensure the best sensing conditions are met[32-34].

Here we present the idea that glycopolymers, glycan analogs that can mimic the activity of a range of molecules, can also serve as useful analogs in nanopore measurements, which allows the ability to understand glycan activity at the single molecule level. We aim to use glycopolymers of different chain length and charge density, and be able to differentiate and selectively detect them using resistive-pulse measurements inside a nanopore. We also aim to test a nanopore's ability to probe the complexation interaction between an anionic glycopolymer and the cationic amino acid, Poly-L-lysine.

RESULTS

The synthetic glycopolymers used in this study carried a pendant galactose ring. Anionic and neutral glycopolymers of different lengths were used. A total of three different synthetic glycopolymers were used in this study. Length was either 30 or 90 residues, and neutral glycopolymers (Gal) had no substitutions on the galactose ring and anionic (Sgal) had one hydroxyl group substituted with a sulfate group, rendering them negatively charged, presumably across all electrolyte pH values used in these experiments. These glyocopolymers will be denoted Gal-30, Sgal-30, and Sgal-90.

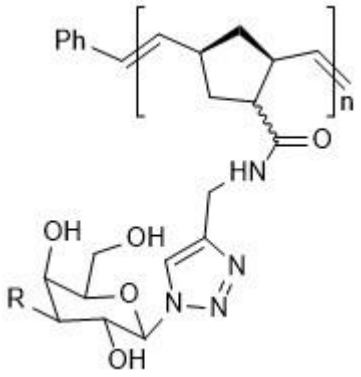

Figure 1: Structure of (S)gal glycopolymers that were synthesized and used during experiments. Polymer length, n = 30 or 90 , R=OH for neutral glycopolymers (Gal-30) and OSO_3^- for anionic glycopolymers (Sgal-30 and Sgal-90).

Nanopores were readily able to detect anionic Sgal-30 and Sgal-90 under a variety of experimental conditions when introduced into the headstage side of the nanopore. In order to correspond with the electrophoretic direction of the molecule through the nanopore, thus promoting analyte movement due to the attraction of a negatively charged glycopolymer to the positively charged electrode in the other electrolyte well, a negative voltage was applied to the headstage side of the nanopore. Initial measurements were taken at 1M KCl, 10 mM HEPES, pH=7, and -200 mV, and 0.2% (w/v) Sgal-30 in water. However, detection at those conditions was deemed suboptimal because analyte sticking on the nanopore surface and blocking of the nanopore was recorded, rendering the nanopore unsuitable for further use. Optimization of the event frequency was completed by systematic changes in experimental conditions, including electrolyte composition and pH, analyte concentration, and applied voltage. The highest event frequency was obtained in 1M KCl, compared to 1M NaCl and 1M LiCl in the same nanopore at pH = 4.3 (the isoelectric point of SiN_x) with analyte concentrations set to 0.2% (w/v),

similar to other glycan measurements such as sodium alginate as performed in the group (See Chapter 1). At this analyte concentration, event frequency was so high that it made data analysis time consuming and difficult, so that analyte concentration was subsequently dropped to 0.02 % (w/v). A similar problem of event frequency was observed with applied voltage, which was thus dropped from -200 mV to -50 mV. The optimization of these parameters was such that event frequency was still sufficiently high so as to enable reasonable (~20 minute) measurement times. After ideal salt and voltage sensing conditions were established, a series of measurements from pH 3 to 7 in increments of 1 pH unit was completed at -50 mV in a ~15 nm diameter nanopore in order to gauge the performance of a nanopore to detect glycopolymers across a wide pH range and to observe its influence on analyte passage through the nanopore . Little analyte sticking was present and when it was present, a ~1.3V "zap" was applied to the nanopore for 50 ms and the current in the nanopore immediately returned to its open pore current. Event frequency declined as a function of pH, most likely due to the change in SiN_x surface charge across the pH range used in the experiment. Given that the isoelectric point of SiN_x is (~4.3±0.3)[35], the SiN_x surface displays a net positive charge below and net negative charge above this point. Being a charged surface, an electrical double layer forms inside the nanopore causing charged counterions (either positive or negative depending on the solution-pH-induced surface charge) from the electrolyte solution to be attracted to the nanopore surface. The thickness of the electrical double layer is dependent on the electrolyte and its concentration, where double layer thickness is inversely proportional to the electrolyte concentration. The involvement of the electrical double layer in the passage of molecules through a nanopore can either enhance or diminish the event characteristics one is looking for by tuning the electroosmotic flow of analyte movement. In our case, competition of electrophoretic and electroosmotic analyte flow at pH=3 caused a slight overall slowing of analyte movement through the nanopore and a superior event frequency was recorded, which is ideal. At pH=3, the nanopore is positively charged, allowing Sgal-30 to become more

attracted to the nanopore entrance and thus also slowing the analyte translocation due to electrostatic attraction of the analyte to the nanopore surface. The near absence of electroosmosis at pH 4 raised the average passage time through the nanopore, however, still at a reasonable event frequency, but lower when compared to pH=3. The teamwork of the two forces above pH 4 greatly decreased the average passage time through the nanopore, seemingly because analyte movement was too quick to detect—often passing through in 10^{-4} to 10^{-5} seconds regardless of electrolyte pH— and a major drop in event frequeny was observed possibly due to instrumental bandwith limitations of 10^{-5} seconds. Nonetheless, we demonstrated that an anionic glycopolymer was able to be detected through a nanopore across a large assortment of experimental conditions, establishing a basis for their continued use in more detailed glycan studies in the future. For each event, the blockage duration, τ, and the fractional blockage current magnitude, $f_b=I/I_0$, was determined with custom event extraction software. A representation of the event characteristics in both τ and f_b at each individual pH measurement is presented in Figure 2.

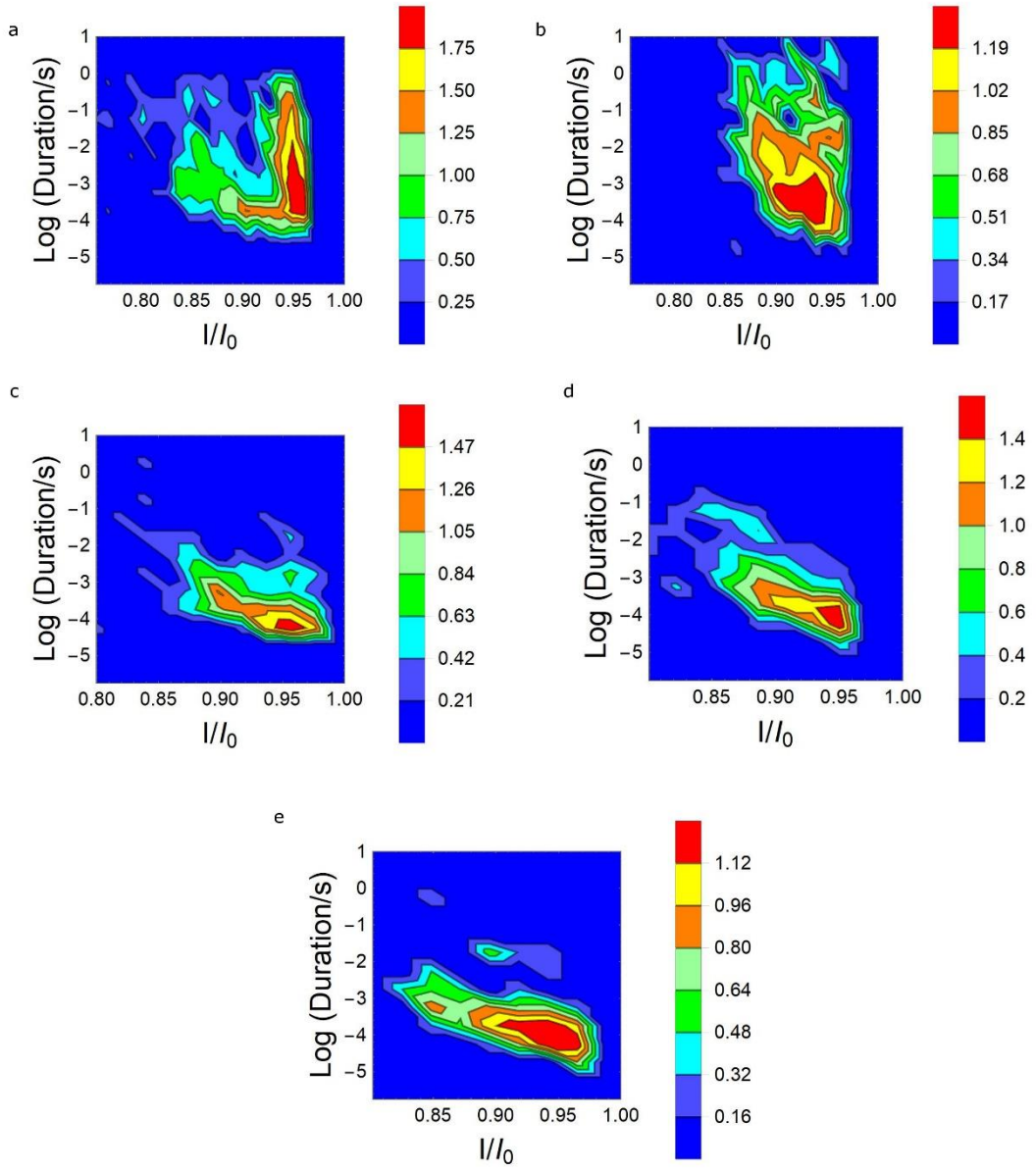

Figure 2: Event counts ($\log_{10}$ of the color axis) of 5uL of 0.02% (w/v) Sgal-30 as a function of 1M KCl, 10 mM HEPES electrolyte pH at -50 mV applied voltage for 30 minutes. a) pH = 3 (1305 events), b) pH = 4 (520 events), c) pH = 5 (223 events), d) pH = 6 (202 events), e) pH = 7 (145 events), through a ~16 nm nanopore. The mode of the event duration decreased with increasing pH as a result of the electroosmotic force corresponding to the electrophoretic direction of analyte movement above pH = 4, causing analyte movement though the nanopore to be faster. 50% of events at or below pH=4 produced durations of 10^{-3} seconds or greater while only 5% of events at or above pH=5 produced similar durations.

Selective detection, defined here as the detection of one specific analyte when more than one is present, of synthetic glycopolymers of different charge in a nanopore was

addressed using Sgal-30 and Gal-30 glycopolymers. A similar experiment was done as described above, where 5 µL of 0.02% (w/v) Gal-30 was run through a ~15nm nanopore for thirty minutes at -50 mV at pH values from 3–7 in increments of one pH unit. The only pH where events were recorded at all for Gal-30 alone was pH 3. At this pH, the nanopore had a positive surface charge and the signal generation direction was consistent with analyte motion by electroosmosis. Events were also recorded at a roughly twenty-four fold lower event frequency (54 events in 30 minutes) when compared to that of Sgal-30 (1305 events) at the same 5 µL aliquot of 0.02% (w/v). Because both Sgal-30 and Gal-30 were independently detected in independent pure samples at pH=3, determining whether or not the two glycopolymers can be differentiated, or even interact with each other was tested by running a 50/50 mixture of Sgal-30 and Gal-30 through the same ~15 nm nanopore (1295 events in 30 minutes). The event characteristics were extracted and analyzed using a conductance-based analysis which histogrammed the drops in nanopore conductance during each individual event. The same analysis was completed for events corresponding to pure Sgal-30 and when compared to that of an Sgal-30-Gal-30 mixture, the conductance based analysis results share similar x-axis positions of the peak maxima as shown in the left hand side of Figure 3. Conductance based analysis on the 54 events that Gal-30 produced at pH=3 conditions had similar characteristics to those of Sgal-30, although the ~20 nS peak was missing, possibly because of the lower total event number. The same experiment and analysis was completed at pH=4, where Sgal-30 can be detected and Gal-30 cannot, and the amount of observable events increased from 521 to 621 after the spiking of 5µL of 0.02% (w/v) Gal-30 into the electrolyte well. However, an independent experiment using 5µL of pure 0.02% (w/v) Gal-30 produced no observable events when injected into the electrolyte well at the same pH and the same nanopore, indicating event frequency increase may have been due to differences in analyte mixing prior to experimentation. Furthermore, observed conductance drops during each individual event presented similar peak maxima and magnitude in the most histogrammed

observed conductance drop, as shown in the right hand side of Figure 3, indicating that the two different synthetic glycopolymers most likely do not interact with each other under pH=4. The peak widths, however, do show intriguing differences between the trials. These differences may arise from the change in surface charge of SiN_x when changing from pH=3 to pH=4, where the nanopore goes from a net positive charge to neutral, which then in turn causes analyte movement through the nanopore to be different. The difference in event behavior as a result of the underlying mechanism that causes analyte movement though the nanopore allows the selective detection of different Sgal-30 and Gal-30 glycopolymers based on their charge if the correct experimental conditions are present (pH=4), and inability to discriminate and selectively detect when they are not (pH=3). Further pH values were not explored due to the low event frequency of Sgal-30 above pH=4.

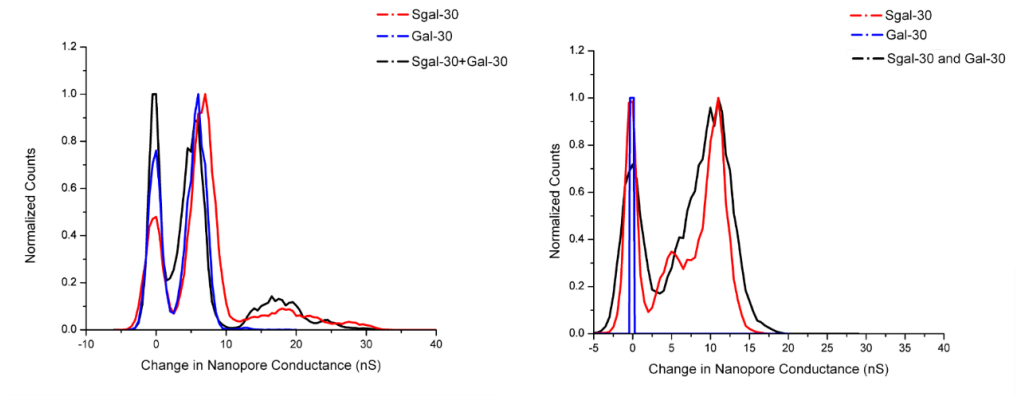

Figure 3: Conductance based analysis of the individual events of Sgal-30, Gal-30, and mixtures of Sgal-30 and Gal-30 in a ~15 nm diameter nanopore at pH=3 (left) and pH=4 (right).

Turning to the question of glycan length discrimination, Sgal-30 and Sgal-90 were readily detected across a variety of conditions, which included changes in analyte concentration, electrolyte concentration, pH, and applied voltage with the hope of being able to differentiate when both glycopolymers were present (Supplementary Figures 2 and 3, Supplementary Table 1). Runs with previously established conditions for Sgal-30, with 1M

KCl, pH=3, and a voltage of -50 mV were able to detect both Sgal-30 and Sgal-90, but didn't afford the ability to clearly differentiate between the two glycopolymers. Although the glycopolymers are different chain lengths, the mechanism of passage through the nanopore may not be shown in the relative current drops during an event, especially if they pass through the pore in a linear fashion due to the inability to distinguish analyte size by f_b values, as Sgal-30 and Sgal-90 should have similar cross sections. Given that that passage speeds of Sgal-30 and Sgal-90 are already fairly fast, they may not be slow enough to distinguish between the two glycopolymers within the bandwidth of the instrumentation. Passage times of glycans in solid-state nanopores appear to be very fast (from past glycan measurements in the group) and are often close to the instrumental bandwidth limitation of 10^{-5} seconds (with the instrument used in this study). The fast nature of glycan movement through a solid-state nanopore may make glycans of different nature appear as if they are the same molecule. In order to enhance the current drops across the nanopore during molecular passage, a salt gradient using 1M KCl in the headstage side and 4M KCl in the ground side at pH = 7, -100 mV was used without attempt to optimize electrolyte pH and applied voltage. Salt gradients have been shown to increase the signal-to-noise ratio in nanopore measurements by increasing the blockage depth during an event by enhancing the electric funneling field near the nanopore entrance[37], a phenomenon that has been under extensive theoretical study[38-39]. Upon using the salt gradient, the event frequency increased by a factor of >10, and increases in the current blockage magnitude were recorded which allowed discrimination between Sgal-30 and Sgal-90. Overall, much larger event depths were recorded for Sgal-90 when compared to the most frequent blockage depths of Sgal-30, and were present in a 50/50 Sgal-30+Sgal-90 mixture.

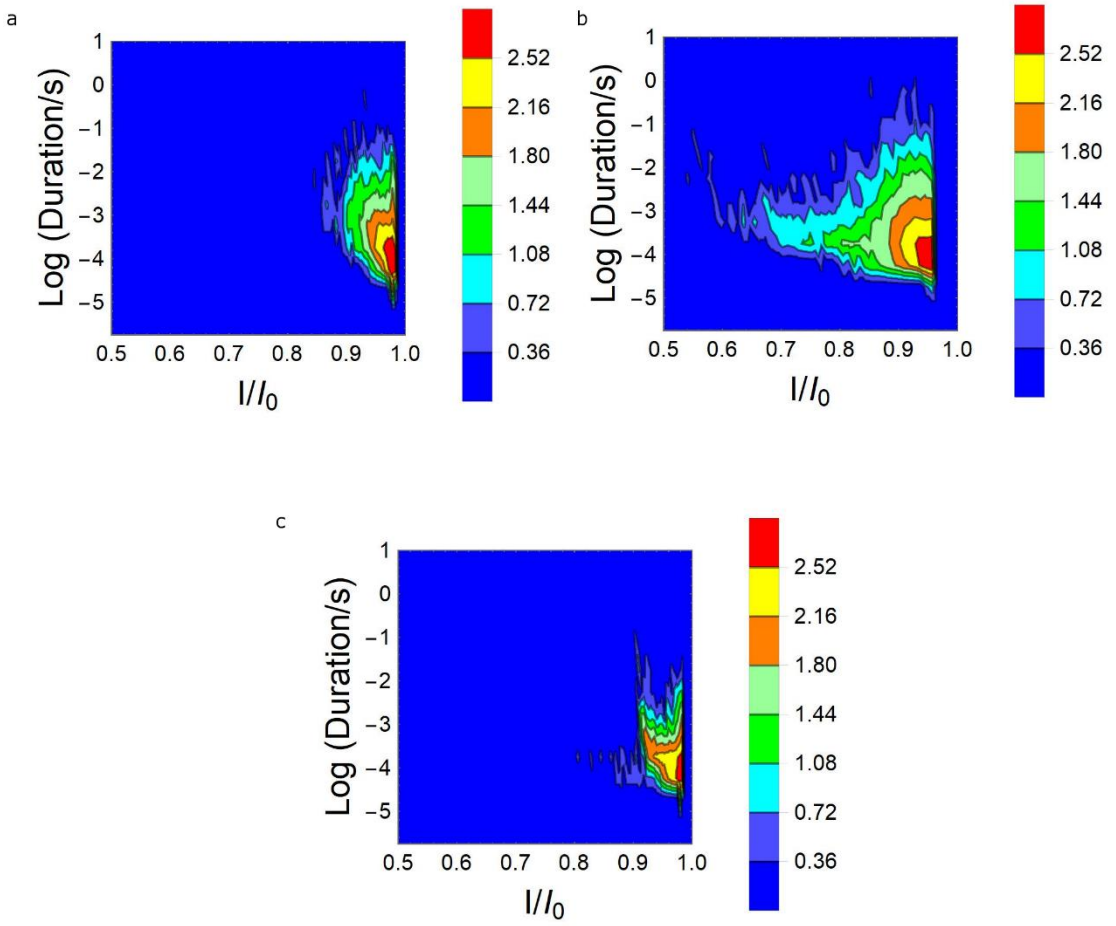

Figure 4: Event counts (log_{10} of the color axis) of 5uL of 0.02% (w/v) a) Sgal-30 (2292 events) b) Sgal-90 (7986 events), and c) a 50/50 mix of 2 µL of Sgal-30 and Sgal-90 (2542 events) in a 1M (headstage) and 4M (ground) salt gradient at -100 mV applied voltage for 5 minutes. Larger events recorded when Sgal-90 was present allows the discrimination between Sgal-30 and Sgal-90.

Given that glycopolymers can serve as analogs in exploring a wide variety of glycan interactions with other molecules, this was put to the test using a cationic polymer, poly-L-lysine, and Sgal-30. Evidence of complexation was revealed in the titration of poly-L-lysine into the nanopore. 5 µL of 0.02% (w/v) Sgal-30 was run through a ~17 nm nanopore using 1M KCl, 10 mM HEPES, pH=3 at -50 mV applied voltage for 10 minutes. After 10 minutes, 1 µL of 0.02% (w/v) poly-L-lysine was added to the headstage side of the nanopore, the same side as Sgal-30, mixed, and the voltage application continued. This experiment was repeated until the total volume of added poly-L-lysine was added reached 3 µL. Event frequency decreased

linearly as a function of added poly-L-lysine, indicating the possibility of a complexation reaction between Sgal-30 and poly-L-lysine while observed nanopore conductance measured with IV curves in between each run stayed constant at ~110 nS suggesting that the nanopore remained unaffected by the addition of the cationic polymer. Control experiments with 5 µL of Sgal-30 over a forty minute span showed no drop in observed event frequency over every ten minute span. A similar experiment was also completed where a previously mixed solution of 0.02% Sgal-30 and 0.02% poly-L-lysine was added into the same pore. Control experiments using pure Sgal-30 produced 790 events over a 30 minute span. A mixture of the respective amount of Sgal-30 and poly-L-lysine only produced 325 events over the same time period, indicating possible complexation between Sgal-30 and poly-L-lysine. Reversal of the voltage polarity to try and detect the formed complex only resulted in small current drops (Supplementary Figure 4) that were able to be distinguished from the baseline, however, without a signal to noise ratio well enough to confidently identify the current drop as an event.

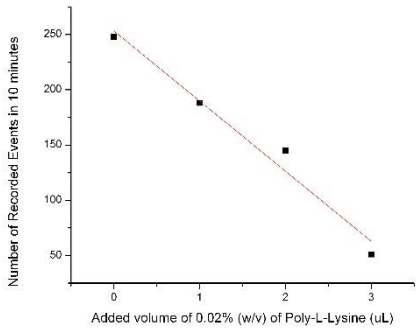

Figure 5: Event frequency plot showing the amount of detectable events of Sgal-30 dropping as a function of added 0.02% (w/v) poly-L-lysine across a ~17 nm nanopore recorded using 1M KCl, pH=3, and -50 mV applied voltage. Event frequency drop indicates possible complexation between the two species.

DISCUSSION

We have demonstrated that solid-state SiN_x nanopores afforded the ability to differentiate between and selectively detect glycopolymers (promising glycan analogs) of varying chain lengths and charge densities, and also the ability to probe the interactions of glycopolymers to form a complex with a cationic amino acid under the right experimental conditions. The known negative charge density of sulfated glycopolymers allowed careful optimization of the experimental process to occur and ideal event behavior to be obtained. The silicon nitride nanopore surface becomes charged when the solution pH deviates from its isoelectric point, and unwanted interactions between the nanopore surface and analyte can arise and analyte sticking to the nanopore can occur frequently. However, simple changes in the experimental acquisition parameters diminished unwanted analyte-nanopore interactions by changing the charge present on the nanopore surface offering us electrostatic control over

analyte capture and translocation. Nanopore sensing of anionic Sgal-30 and Sgal-90 glycopolymers was accomplished over a wide range of electrolyte types and pH values, and event frequency distributions were obtained as a function of pH allowing for optimal electrolyte pH for detection to be established (Figure 2, Supplemetary Figures 2 and 3, and Supplementary Table 1). Selective detection of glycopolymer Sgal-30 versus Gal-30 was accomplished by simple changes in electrolyte pH under particular conditions (pH=4) presumably arising from their charge differences. The attraction of a charged ion in direct response to an applied electric field, electrophoresis, appears to serve as the main driving force behind analyte movement through the nanopore for all anionic glycopolymers used in this study. The introduction of a salt gradient also allowed the discrimination between glycopolymers of different lengths, where measurements done without salt gradients failed to produce definitive evidence to indicate that the two different chain length glycopolymers were different from each other.

Understanding the surface chemistry of SiN_x as a function of both electrolyte pH and concentration allowed for glycopolymer detectionoptimization. The ability to tune the SiN_x surface charge from negative to neutral at the isoelectric point to positive allowed the tuning of electrostatic interactions and phenomena such as electroosmosis. It is clear in the case of Sgal-30 that when electrophoretic and electroosmotic directions are the same, analyte flow through a nanopore appears extremely fast and possibly undetectable using conventional measuring devices because of their bandwidth limitations. At pH=5 and above, roughly 5% of the recorded events produced durations of 10^{-3} seconds or longer. On the contrary, analyte movement through a nanopore is slowed when electrophoresis and electroosmosis oppose each other, allowing for more effective and selective glycopolymer detection. At pH=3 and 4, over 50% of the recorded events were longer than 10^{-3} seconds (See supplementary Figure 5.

We hope that these initial nanopore measurements with glycopolymers may lead to more detailed studies of their possible interactions with a variety of molecules.

METHODS

A full listing of the experimental details is available in the Supplementary Information. Nanopores were formed via dielectric breakdown[40] in nominally 10 nm-thick silicon nitride (SiN_x) membranes. Nanopore sizes were inferred from their conductance, *G*, determined from Ohmic current-voltage data assuming a cylindrical nanopore shape and bulk and surface conductances. Nanopores used for measurements produced stable open-pore (analyte-free) currents in the electrolyte solutions used. Glycopolymers were made by Blais Leeber from Brown University from the group of Amit Basu. For routine measurements, sample aliquots were added to the headstage side (Figure 1), leaving the ground side free of initially added analyte. Current blockages were extracted using a current-threshold analysis. All applied voltages are stated with the polarity of the electrode on the headstage side relative to ground on the ground side of the sample cell (As shown in Supplementary Figure 1).

AUTHOR INFORMATION

Corresponding Author

Email: jason_dwyer@uri.edu

Author Contributions

All authors have contributed to, and approve, the manuscript.

Acknowledgements

This research has been supported by NSF CAREER award CBET-1150085 and a 2017 RI Science and Technology Advisory Council Award

REFERENCES

1. Kwon, D. S., Gregorio, G., Bitton, N., Hendrickson, W. A. & Littman, D. R. DC-SIGN-Mediated Internalization of HIV Is Required for Trans-Enhancement of T Cell Infection. *Immunity* **16,**135–144 (2002).
2. Kooyk, Y. V. & Rabinovich, G. A. Protein-glycan interactions in the control of innate and adaptive immune responses. *Nature Immunology* **9,**593–601 (2008).
3. Puffer, E. B., Pontrello, J. K., Hollenbeck, J. J., Kink, J. A. & Kiessling, L. L. Activating B Cell Signaling with Defined Multivalent Ligands. *ACS Chemical Biology* **2,**252–262 (2007).
4. Collins, B. E. *et al.*High-Affinity Ligand Probes of CD22 Overcome the Threshold Set by cis Ligands to Allow for Binding, Endocytosis, and Killing of B Cells. *The Journal of Immunology* **177,** 2994–3003 (2006).
5. Collins, B. E. *et al.*Masking of CD22 by cis ligands does not prevent redistribution of CD22 to sites of cell contact. *Proceedings of the National Academy of Sciences* **101,** 6104–6109 (2004).
6. Rabinovich, G. A., Kooyk, Y. V. & Cobb, B. A. Glycobiology of immune responses. *Annals of the New York Academy of Sciences* **1253 ,** 1–15 (2012).
7. Varki, A. Biological roles of oligosaccharides: all of the theories are correct. *Glycobiology* **3,** 97–130 (1993).
8. Dalziel, M., Crispin, M., Scanlan, C.N., Zitzmann, N. & Dwek, R.A. Emerging Principles for the Therapeutic Exploitation of Glycosylation. *Science* **334**, 75-79 (2011).
9. Ernst, B. & Magnani, J.L. From carbohydrate leads to glycomimetic drugs. *Nat Rev Drug Discov* **8**, 661-677 (2009).
10. Pinho, S.S. & Reis, C.A. Glycosylation in cancer: mechanisms and clinical implications. *Nat Rev Cancer* **15**, 540-555 (2015).
11. World Health Organization (2017, August). WHO Model List of Essential Medicines 20th List. Retrieved from http://www.who.int/medicines/publications/essentialmedicines/en/
12. Szajek, A.Y., Chess, E., Johansen, K., Gratzl, G., Gray, E., Keire, D., Linhardt, R. J., Liu, J., Morris, T., Mulloy, B., Nasr, M., Shriver, Z., Torralba, P., Viskov, C., Williams, R., Woodcock, J., Workman, W., Al-Hakim, A. The US regulatory and pharmacopeia response to the global heparin contamination crisis. *Nature Biotechnology* **34**, 625–630 (2016)
13. Liu, H., Zhang, Z. & Linhardt, R.J. Lessons learned from the contamination of heparin. *Natural Product Reports* **26**, 313-321 (2009).
14. Karawdeniya, B. I., Bandara, Y. M. Nuwan D. Y., Nichols, J. W., Chevalier, R. B., , and Dwyer, J. R., Tasty, Therapeutic, or Toxic? Gauging Thin-Film Solid-State Nanopores for Polysaccharide Sensing. Nature Commun. 2018 *Under Revision*
15. Haywood, D.G., Saha-Shah, A., Baker, L.A. & Jacobson, S.C. Fundamental Studies of Nanofluidics: Nanopores, Nanochannels, and Nanopipets. *Anal. Chem.* **87**, 172-187 (2015).
16. Taniguchi, M. Selective Multidetection Using Nanopores. *Anal. Chem.* **87**, 188-199 (2015).
17. Reiner, J.E. et al. Disease Detection and Management via Single Nanopore-Based Sensors. *Chem. Rev.* **112**, 6431-6451 (2012).
18. Howorka, S. & Siwy, Z. Nanopore analytics: sensing of single molecules. *Chem. Soc. Rev.* **38**, 2360-2384 (2009).

19. Miles, B.N. et al. Single Molecule Sensing with Solid-State Nanopores: Novel Materials, Methods, and Applications. *Chem. Soc. Rev.* **42**, 15-28 (2013).
20. Oukhaled, A., Bacri, L., Pastoriza-Gallego, M., Betton, J.-M. & Pelta, J. Sensing Proteins through Nanopores: Fundamental to Applications. *ACS Chemical Biology* **7**, 1935-1949 (2012).
21. Branton, D. et al. The potential and challenges of nanopore sequencing. *Nat. Biotechnol.* **26**, 1146-1153 (2008).
22. Oh, Y. I., Sheng, G. J., Chang, S.-K. & Hsieh-Wilson, L. C. Tailored Glycopolymers as Anticoagulant Heparin Mimetics. *Angewandte Chemie* **125,**12012–12015 (2013).
23. Kiessling, L. L. & Grim, J. C. ChemInform Abstract: Glycopolymer Probes of Signal Transduction. ChemInform 44, (2013).
24. Ting, S. R. S., Chen, G. & Stenzel, M. H. ChemInform Abstract: Synthesis of Glycopolymers and Their Multivalent Recognitions with Lectins. *ChemInform* **42,** (2011).
25. Qiu, S., Huang, H., Dai, X.-H., Zhou, W. & Dong, C.-M. Star-shaped polypeptide/glycopolymer biohybrids: Synthesis, self-assembly, biomolecular recognition, and controlled drug release behavior. *Journal of Polymer Science Part A: Polymer Chemistry* **47,** 2009–2023 (2009).
26. Wang, L.-X. Faculty of 1000 evaluation for Noncarbohydrate glycomimetics and glycoprotein surrogates as DC-SIGN antagonists and agonists. *F1000 - Post-publication peer review of the biomedical literature e* (2013).
27. Bacri, L. et al. Discrimination of neutral oligosaccharides through a nanopore. *Biochem. Biophys. Res. Commun.* **412**, 561-564 (2011).
28. Fennouri, A. et al. Single Molecule Detection of Glycosaminoglycan Hyaluronic Acid Oligosaccharides and Depolymerization Enzyme Activity Using a Protein Nanopore. *ACS Nano* **6**, 9672-9678 (2012).
29. Fennouri, A. et al. Kinetics of Enzymatic Degradation of High Molecular Weight Polysaccharides through a Nanopore: Experiments and Data-Modeling. *Anal. Chem.* **85**, 8488-8492 (2013).
30. Kullman, L., Winterhalter, M. & Bezrukov, S.M. Transport of Maltodextrins through Maltoporin: A Single-Channel Study. *Biophys. J.* **82**, 803-812 (2002).
31. Zhao, S. et al. Sugar-stimulated robust nanodevice: 4-Carboxyphenylboronic acid modified single glass conical nanopores. *Electrochem. Commun.* **36**, 71-74 (2013).
32. *Wanunu, N., Meller, A. Chemically Modified Solid-State Nanopores. Nano Lett **7** **(6),*** 1580–1585 (2007)
33. Hoogerheide, D.P., Garaj, S., Golovchenko, J.A. Probing surface charge fluctuations with solid-state nanopores. Phys. Rev. Lett. 102 (25), 256804 (2009)
34. Guo, W., Tian, Y., Jiang, L. Asymmetric Ion Transport through Ion-Channel-Mimetic Solid-State Nanopores *Acc. Chem. Res. **46*** **(12),** 2834–2846 (2013)
35. Okoth, R., Basu, A. End-labeled amino terminated monotelechelic glycopolymers generated by ROMP and Cu(I)-catalyzed azide–alkyne cycloaddition *Beilstein J. Org. Chem.* **9**, 608–612 (2013).
36. Hoogerheide, D.P., Garaj, S. & Golovchenko, J.A. Probing Surface Charge Fluctuations with Solid-State Nanopores. *Phys. Rev. Lett.* **102**, 256804 (2009)
37. Reiner, J. E., Kasianowicz, J. J., Nablo, B. J. & Robertson, J. W. F. Theory for polymer analysis using nanopore-based single-molecule mass spectrometry. *Proceedings of the National Academy of Sciences* **107,** 12080–12085 (2010).

38. Hatlo, M. M., Panja, D. & Roij, R. V. Translocation of DNA Molecules through Nanopores with Salt Gradients: The Role of Osmotic Flow. *Physical Review Letters* **107,**(2011).
39. He, Y. *et al.*Mechanism of How Salt-Gradient-Induced Charges Affect the Translocation of DNA Molecules through a Nanopore. *Biophysical Journal* **105,**776–782 (2013).
40. Hsu, J.-P., Yang, S.-T., Lin, C.-Y. & Tseng, S. Ionic Current Rectification in a Conical Nanopore: Influences of Electroosmotic Flow and Type of Salt. *The Journal of Physical Chemistry C* **121,**4576–4582 (2017).
41. Kwok, H., Briggs, K. & Tabard-Cossa, V. Nanopore Fabrication by Controlled Dielectric Breakdown. *PLoS ONE* **9**, e92880 (2014).

APPENDICES

Supplementary Information

Tasty, Therapeutic, or Toxic? Gauging Thin-Film Solid-State Nanopores for Polysaccharide Sensing

Buddini Iroshika Karawdeniya, Y.M. Nuwan D.Y. Bandara, Jonathan W. Nichols, Robert B. Chevalier, and Jason R. Dwyer

Department of Chemistry, University of Rhode Island, 140 Flagg Road, Kingston, 02881, USA.

Reagents and Materials.

The following materials, identified by their product number and specification, were obtained from Sigma-Aldrich Corporation (St. Louis, MO, USA): Potassium chloride (60130, puriss. p.a., ≥99.5% (AT)); HEPES potassium salt (H0527, ≥99.5% (titration)); sulphuric acid (339741, 99.999%); alginate lyase (A1603, ≥10,000 units/g); and hydrochloric acid (320331, ACS reagent, 37%). Polysaccharides were commercially obtained: sodium alginate A1-B25266 (~75-120 kDa, 40-90 centipoise (1% solution); Alfa Aesar [Ward Hill, MA, USA]) and A2- PROTANAL® LFR5/60 (120kDa, 300-700 centipoise (10% solution); FMC

Corporation Health and Nutrition, PA, USA); heparin sodium salt (USP, 1304038, Rockville, MD) and over sulfated chondroitin sulfate (OSCS) (USP, 1133580) from Sigma Aldrich Corporation (St. Louis, MO, USA). The potency of the USP heparin samples was 180 USP heparin units according to Pharmacopeial Forum Vol. 35(5) [Sept.–Oct. 2009].

Silicon-rich LPCVD silicon nitride (nominally) 10 nm-thick membranes on 200 μm-thick silicon frame (NT001Z and NT005Z; with reported membrane thicknesses for Lot # L8 10.5±0.3 nm, L15 16±2 nm, L31 14±2 nm, L68 12±2 nm) were purchased from Norcada, Inc. (Alberta, Canada).

All aqueous solutions were prepared using Type I water (~18 MΩ·cm resistivity from either a Millipore Synergy UV [Billerica, MA], or American Aqua Maxicab system [Narragansett, RI, USA]); all dilutions and washes also used this water. Stericup-VP vacuum filtration systems were used to filter electrolyte solutions after preparation, and water to prepare alginate solutions (SCVPU11RE 0.10 μm pore size in polyethersulfone membrane; EMD Millipore Corporation [MA, USA]).

Ag/AgCl electrodes were made from 1.0 mm-diameter silver wire (Alfa Aesar 11434, annealed, 99.9% (metals basis)) by soaking overnight in sodium hypochlorite (Alfa Aesar 33369, 11-15% available chlorine). Electrodes were insulated using shrink-wrap PTFE tubing (McMaster-Carr, 7960K21, high-temperature harsh environment tubing, moisture seal, heat-shrink, 0.07" ID before; and 7564K67, high-temperature harsh environment tubing, heat-shrink, 0.08" ID before, 0.05" ID after) and connected to electronics using pins (Connectivity TE Connectivity / AMP 205090-1 D sub circular connector contact, AMPLIMITE 109 Series, Socket, Crimp, 20-24 AWG). Nanopore chips were compressed between silicone gaskets (McMaster-Carr, 86435K43, high-temperature silicone rubber sheet, ultra-thin, 12" x 12", 0.015" thick, 35A durometer) in custom-machined PTFE holders with ~500 μL sample wells.[1]

Silicone tubing with ID 1.0 mm x OD 3.0 mm was obtained from Nanion Technologies GmbH, Munich, Germany.

Instrumental Details.

Measurements of solution pH and conductivity were with an Orion Star™ pH meter and Orion™ ROSS Ultra™ Refillable pH/ATC Triode™ Combination Electrodes and Orion™ DuraProbe™ 4-Electrode Conductivity Cells (Thermo Fisher Scientific Inc, MA, USA).

Nanopore formation by dielectric breakdown was performed using programmable DC power supplies (Model 9121A, B&K Precision Corporation, CA, USA) interfaced to a home-built circuit;[2] real-time current measurements were by a 428-Programmable Current Amplifier (Keithley Instruments, Cleveland, OH, USA) interfaced to NI USB 6351 DAQ card using LabView-based (National Instruments Corp., TX, USA) software to control the applied voltage.

All nanopore measurements were performed using an Axopatch 200B amplifier (Axon Instruments, Foster City, CA, USA) in voltage clamp mode. The amplifier was interfaced to a computer system using a data acquisition card (779512-01 NI PCIE-6251 M Series with 777960-01 NI BNC-2120 shielded connector block) and control software written in LabView. Current-versus-time measurements were typically acquired for 1 h (3× 20 min) at 100 kHz acquisition rates with the 4-pole low pass Bessel filter built-in to the Axopatch 200B set to 10 kHz. Measurements of nanopore conductance were acquired at a rate of 10 kHz, with the filter set to 1 kHz.

Infrared spectra of the powder were acquired by FTIR-ATR (Bruker Tensor 27 equipped with a Ge crystal) averaged over 256 scans with 4 cm^{-1} spectral resolution. All measurements done inside a nitrogen filled glovebox.

UV/Vis spectra were collected using a Varian Cary 50 Bio UV/Visible Spectrophotometer with a quartz cuvette with a 1 cm pathlength. Single run measurements were taken from 200 to 400 nm at a scan rate of 300 nm/min and 0.50 nm intervals.

All 3D printed components were designed in Solid Works 2014 Professional Edition (Dassault Systems SolidWorks Corporation, Waltham, MA) and printed by Makerbot Replicator (MakerBot Industries, Brooklyn, NY) using PLA plastic (MP06103, MakerBot Industries, Brooklyn, NY).

General procedure.

Nanopores in the ~10 nm-thick silicon nitride membranes were fabricated by controlled dielectric breakdown using 11-15.5 V DC applied potentials.[2] The nanopore formation was carried out in 1 M KCl electrolyte, HEPES-buffered to pH ~7, and the membranes and pores were secured in custom-machined PTFE holders with ~500 μL sample wells.

Nanopore conductances, *G*, were the slope of the fit to the experimental Ohmic current-voltage data, measured in 1 M KCl electrolyte buffered with HEPES at pH ~7. The corresponding nominal nanopore diameters were calculated using a conductance model (including bulk, surface, and access resistance terms) and cylindrical nanopore shape suitable for this salt concentration and fabrication method, $G = \left(\frac{1}{G_{\text{bulk}}+G_{\text{surface}}} + \frac{1}{G_{\text{access}}}\right)^{-1}$.[2-5] Nanopores used for measurements produced stable open-pore (analyte-free) currents at the salt concentrations used.

All electrolyte solutions were HEPES-buffered (10 mM) to pH ~7 (adjusted with dropwise addition of concentrated hydrochloric acid), and measurements were carried out using filtered solutions with 0.1, 1.0, and 4.0 M KCl concentrations. Solutions of 0.2% (w/v)

sodium alginate, 0.2% (w/v) heparin, and 0.2% (w/v) OSCS were made by dissolving the solids in filtered Type I water. For routine measurements and unless otherwise specified, 4 μL aliquots were added to the headstage side (Figure 1), leaving the ground side free of initially added analyte. Calibration curves for each nanopore were constructed by repeated cycles of measurement followed by the addition of another analyte aliquot. Current blockages were extracted using a current-threshold analysis. Any current blockages exceeding 100 s ($\lesssim 0.1\%$) were not included in analyses.

Polysaccharide Viscosity Measurements.

Apparent viscosity measurements were carried out on aqueous sodium alginate solutions (0.15-1.0 g/dL) in 0.1 M sodium chloride solutions using a capillary viscometer (SI Analytics Ubbelohde Viscometer, Thermo Fisher Scientific, Inc., MA, USA) immersed in a thermostatted bath at 23°C. Triplicate measurements of the apparent viscosity were made at each solution concentration to yield the intrinsic viscosity, [η], from[6]

$$\frac{\eta_{\text{sp}}}{C} = [\eta] + k[\eta]^2 C$$

where C is the macromolecule's concentration in g/dL, k is a constant characteristic of the solute-solvent system, $\eta_{\text{sp}} = \frac{\eta_{\text{solution}}}{\eta_{\text{solvent}}} - 1$ is the specific viscosity calculated from the apparent viscosities. The weight- and number-average molecular masses, M_{w} and M_{n}, and the of the polymers in kDa were calculated according to[8]

$$[\eta] = 0.023(M_{\text{w}})^{0.984}$$

$[\eta] = 0.095(M_{\text{n}})^{0.963}$.

The respective molecular masses of the two alginate samples were determined by this method to be 286 kDa and ~74 kDa for *A1*, and 71 kDa and 18 kDa for *A2*. Using a polymer's molecular weight, M, we can calculate the hydrodynamic radius (N_{A} is Avogadro's number)[9]

$$R_{\text{h}} = \left(\frac{3[\eta]M}{10\pi N_{\text{A}}}\right)^{1/3}$$

to be ~19 nm for *A1* and ~8 nm for *A2* (on an M_{n}-basis). The corresponding root-mean-squared end-to-end distance, $\langle\overline{r^2}\rangle^{1/2}$ for each sample is equal to $3.1R_{\text{h}}$.

Acid and Enzymatic Digestion Procedures.

A ~9 nm nanopore was mounted in the PTFE sample holder. A 200 μL amount of 0.2% (w/v) *A1* was added to the head stage side in 5 μL aliquots per hour throughout the work day during 4 days of application of a +200 mV cross-membrane voltage. For overnight voltage applications, the electrode polarity was maintained, but the electrodes were placed in the opposite wells. The head-stage and initially analyte-free ground side solutions were extracted, individually mixed with 1 mL of 75% sulphuric acid and heated overnight (16 h) at 80°C. Samples were diluted with 3 mL of water before spectral acquisition.

A 2250 μL aliquot of 0.2% (w/v) *A1* was added to a 150 μL aliquot of 1 unit/mL alginate lyase and heated in a water bath at 37˚C for 30 minutes. Samples of 3% (w/v) *A2* were mixed with alginate lyase (1:1 (v/v) mixture with 1 unit/mL enzyme) for 10 minutes at 37°C. 20 μL of this mixture was added to the headstage side and events were detected with the application of +200 mV on the head stage side. Measurements in the presence of 20 μL of 1 unit/mL of alginate lyase, alone, in the headstage side support that the detected events in the presence of analyte originated from enzymatic digestion products.

Preparation of Heat Maps by Histogramming Individual Events.

Heat maps were prepared in Origin (Originlab Corporation, MA) from event data sorted into bins by paired f_b and τ. The bin width along the f_b axis was set equal to $3.49\sigma(f_b)N^{-\frac{1}{3}}$, where $\sigma(f_b)$ is the standard deviation across all events, and N is the total number of events.[9] Bin size along the τ axis was set to $\sqrt{10}$. Heat maps are plotted using $\log_{10}$ of the number of events in each bin.

Recognition Flag Generation

Recognition flag generation was done using custom codes written in Mathematica 11.0.1.0 (Wolfram, Champaign, IL). (1) All individual events were histogrammed with respect

to f_b using a bin width of 0.0025 (using nanopores with diameters from ~8-14 nm, and determined using the USP heparin data). (2) Any bin with counts below 0.5% of the maximum bin count were removed, and all counts were then normalized. (3) The OSCS identification threshold was taken to be at the nearest bin at the distance of three standard deviations (after the 0.5% filter) from the bin with the maximum number of counts. (4) When events had been detected at f_b below this threshold, the recognition flag was set to red to signal the presence of OSCS; it was otherwise left white.

(5) All individual events were then histogrammed with respect to the logarithm ($\log_{10}$) of the event duration (τ) using a bin width of 0.25 (here, determined using the USP OSCS data). (6) The same 0.5% filter was applied to these histograms, which then had their counts normalized. (7) The event duration threshold was taken to be the nearest bin at the distance of three standard deviations (after the 0.5% filter) from the bin with the maximum number of counts. (8) When events had been detected at $\log_{10}\tau$ above this threshold, the recognition flag was set to red to signal the presence of heparin; it was otherwise left white.

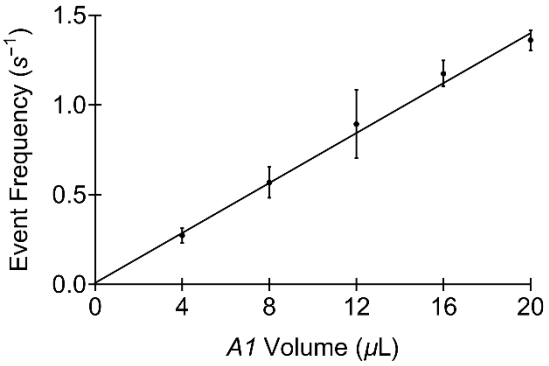

Supplementary Figure 1: Calibration curve of sodium alginate event frequency versus volume of 0.2% (w/v) *A1*. Two trials were performed, with each data point including at least 1000 events extracted from at least 1 h long measurements at 200 mV applied voltage after consecutive additions of 4 µL aliquots to the headstage side of the same nanopore. Error bars represent the standard deviation across the trials.

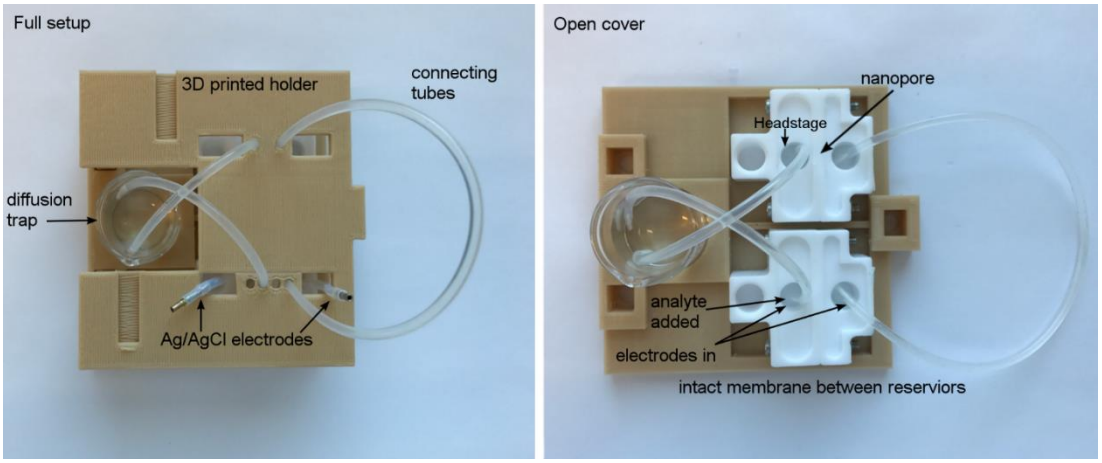

Supplementary Figure 2: A special nanopore configuration in which the electrolyte wells proximal to the electrodes and to the nanopore were physically separated. The purpose of this configuration was to determine if the current blockages arose from analyte interaction with the electrodes, or with the nanopore, itself. The electrolyte wells in the lower PTFE cell held the electrodes and were separated by an intact SiN_x membrane that did not allow ionic flow. These wells were connected through electrolyte-filled silicone tubing and an electrolyte-filled beaker, to a second electrolyte-filled PTFE cell in which the wells were separated by a SiN_x nanopore. With analyte injected into the bottom cell, the only possible mechanism of current blockage was either by direct interaction with the electrodes, or by the passage of analyte through the tubing and beaker of solution until it could interact with the nanopore. When a 4 µL aliquot of the alginate was added to the head stage side of the lower cell, only 18 appreciable current transients were detected in a 1 hour measuring period, contrasted with 561 events in 1 hour when the alginate was directly injected adjacent to the head stage side of the nanopore. The additional electrolyte between electrodes and nanopore reduces the cross-pore applied potential compared to the usual single-cell sensing configuration.

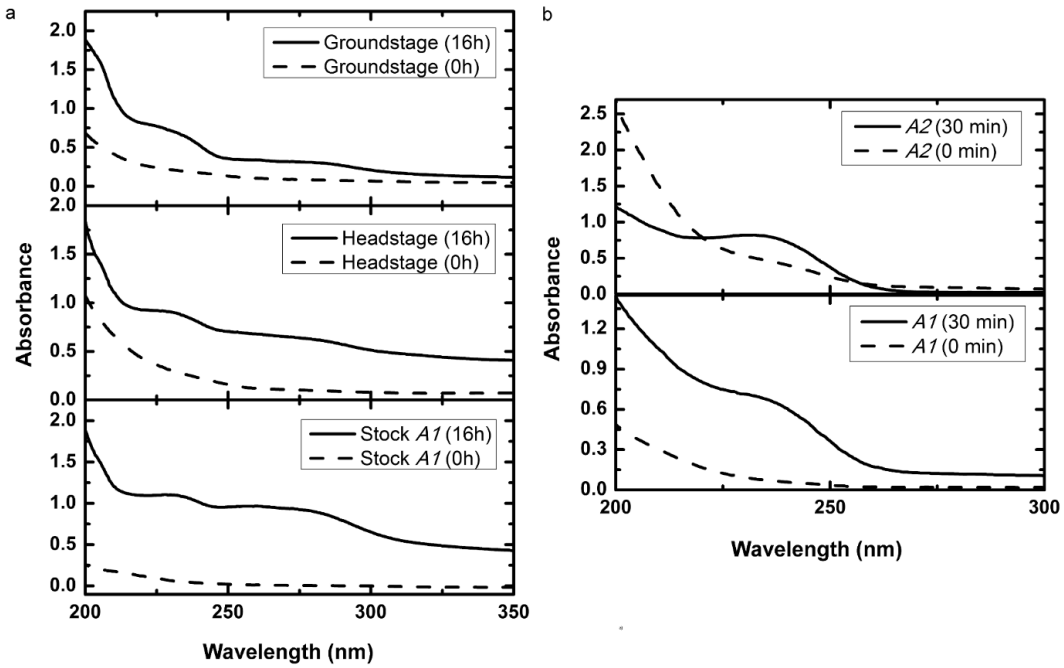

Supplementary Figure 3. UV/Vis spectra of acid and enzymatic digestion products. a) Stock *A1* subjected to 16 h of sulphuric acid digestion generated a UV/Vis spectrum characteristic of the digested polysaccharide[10, 11] that was replicated in the samples taken from the headstage and from the groundstage sample wells after 4 days of a translocation experiment (200 µL aliquot). The dashed lines denote the UV/Vis spectra of the sample before digestion, and the solid lines denote the spectra after digestion. b) Alginate lyase digestion of alginate is expected to introduce chromophores with a peak absorption at ~232 nm, consistent with observations here.[12]

Preparation of Heat Maps by Histogramming Individual Events.

Heat maps were prepared in Origin (Originlab Corporation, MA) from event data sorted into bins by paired f_b and τ. The bin width along the f_b axis was set equal to $W_{bin} = 3.49\sigma(f_b)N^{-1/3}$, where $\sigma(f_b)$ is the standard deviation across all events, and N is the total number of events.[13] Bin size along the τ axis was set to $\sqrt{10}$. Heat maps are plotted using $\log_{10}$ of the number of events in each bin.

The distributions of event counts by f_b in Supplementary Figure 4 were fit using the function

$$\phi_{f_b} = \frac{1}{2}(1+\theta)\sum_{i=1}^{M} A_i \cdot \exp\left(-\frac{(f_b-\mu_i)^2}{2\sigma_i^2}\right)$$

where the parameters of the unmodified Gaussian function are as conventional -A_i, μ_i, and σ_i are the magnitude scaling, expected value, and standard deviation. The step function, $(1+\theta)$ was set to 1 for $f_b < f_b^{cutoff} + W_{bin}$ and 0 otherwise, so that the fit function covers only the accessible experimental data (f_b^{cutoff} was the threshold for event extraction). The fit parameters were

Panel	A_1	μ_1	σ_1
a	364 A_2=76	0.971 μ_2=0.773	0.0624 σ_2=0.0992
b	240	0.991	0.00274
c	150	0.98	0.00558
d	100 A_2=304	0.974 μ_2=0.979	0.0041 σ_2=0.002
e	312	0.991	0.00635
f	500 A_2=2120	0.985 μ_2= 0.989	0.0077 σ_2=0.0016

The distributions of the log of event counts by duration were fit to a log-normal distribution

$$\phi_\tau = \frac{A}{\tau} e^{-(\ln \tau - M)^2/(2S^2)}$$

where the parameters had conventional meanings, and the event duration was expressed in μs. The event duration corresponding to the peak of the event count distribution, τ_p , was found by taking the first derivative of the curve.

Panel	A	M	S	τ_p (μs)
a	5.49	1.01	0.57	98.91
b	5.93	1.07	0.55	143.98
c	6.95	1.38	0.51	1102.32
d	5.43	1.11	0.67	89.31
e	6.62	1.15	0.55	218.69
f	6.85	0.81	0.50	57.27

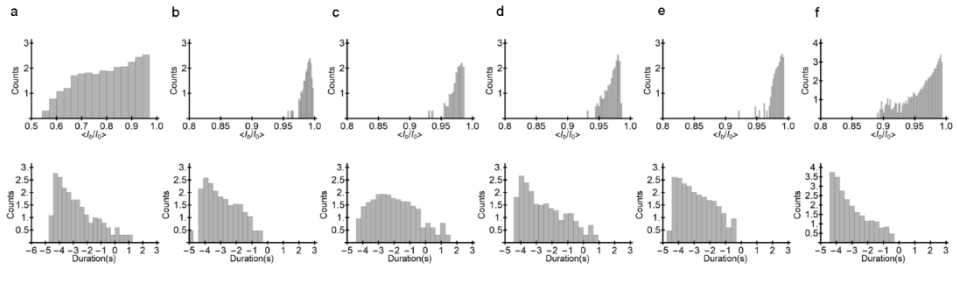

Supplementary Figure 4: Histograms of (top row) $\langle i_b \rangle / \langle i_0 \rangle$ (bottom row) duration in $\log_{10}$ of *A1* alginate in (a) ~5 nm and (b) ~19 nm pore, *A2* in (c) ~22 nm, (d) 10-min enzyme digested *A2* in ~23 nm pore, (e) heparin and (f) OSCS in the same ~14 nm pore with the bin size set automatically by the measurement statistics as described above.

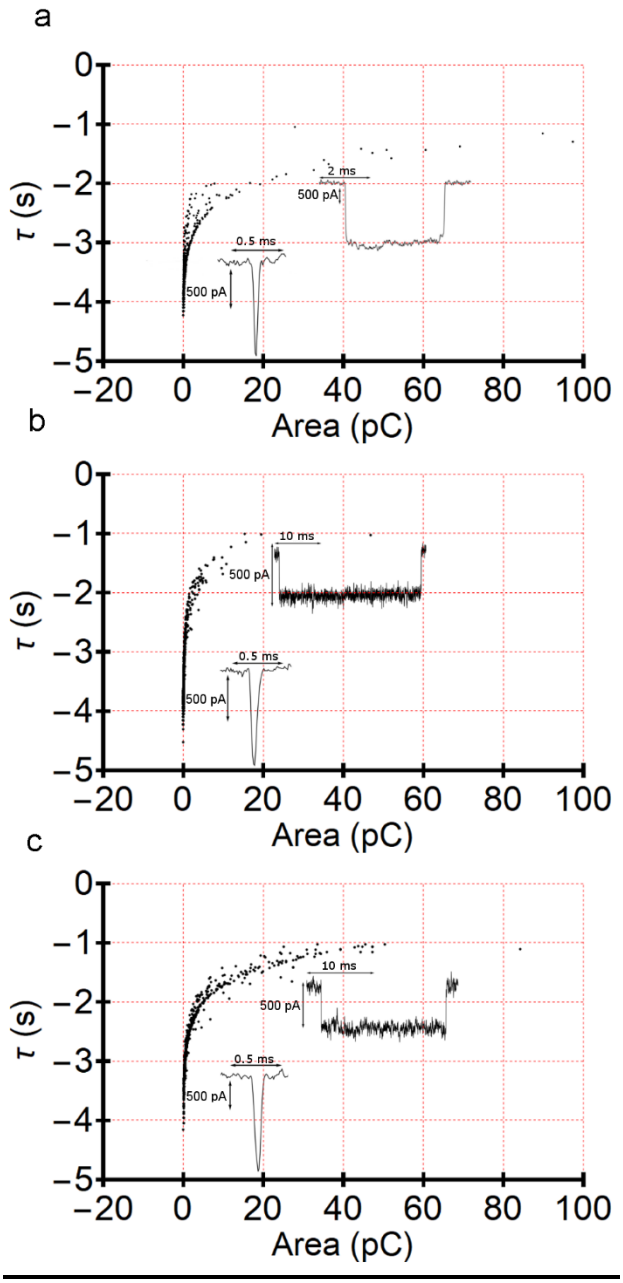

Supplementary Figure 5: Plots of $\log_{10}$ of event duration (τ) versus area under each event for alginate *A1* in a) ~5 nm and b) ~19 nm diameter pores and c) for alginate *A2* in a ~22 nm diameter pore recorded for 1 hour in 1 M KCl at pH ~7. Two distinct event distribution tails are visible corresponding to short-lived spike-like pulses and longer-lived rectangular blockages. The longer-lived tail for *A2* is more prominent as a percentage of total events than for *A1*, consistent with the appearance of the combined heat and scatter plots in Figure 3. The shorter events could be attributed to either "bumps" or fast translocations, and longer-lived events could be attributed to slower translocations or longer-lived interactions with the pore (in both cases, complementary measurements independently confirmed alginate translocation). The low molecular weight and high M/G ratio (more G is attributed to stiffness) of A2 meant, it has a greater probability of

translocating through a given pore hence tails seen in the figure above are not surprising. Area under each event was calculated by integrating the interpolation function (interpolation order of 1) of each event in Mathematica.

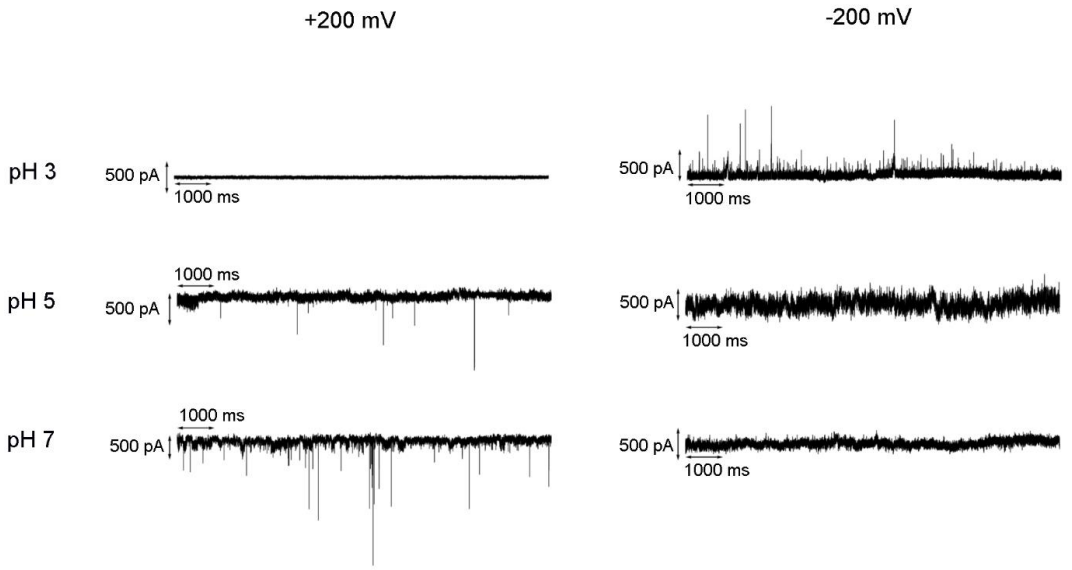

Supplementary Figure 6. Representative current events of *A1* alginate at pH 3,5 and 7 at negative and positive 200 mV applied on the head stage side for 1-hour each in the same 8 nm diameter pore at 1M KCl.

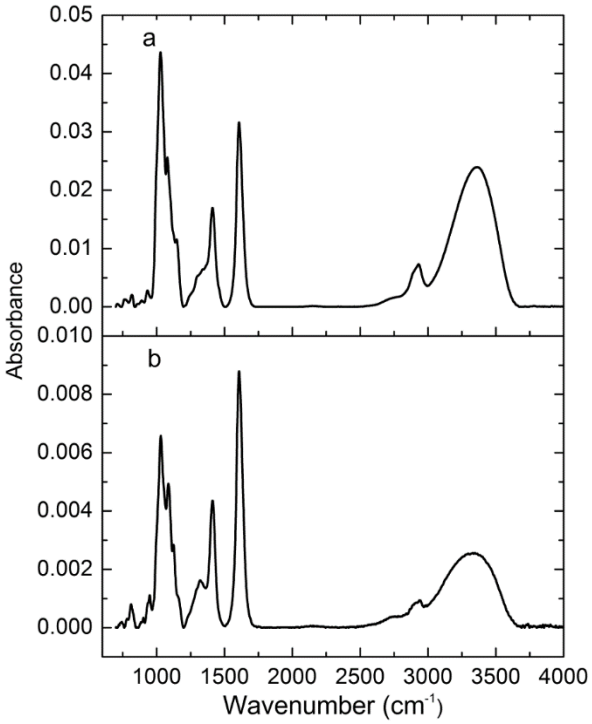

Supplementary Figure 7. Infrared spectra of alginate samples. The intensity of the peaks near 1400 and 1600 cm^{-1}, relative to the remainder of the spectrum, are consistent with a lesser proportion of carboxylic acid salt residues in (a) *A1* than in (b) *A2*. Comparison of the intensity of the guluronic (G) unit absorption at ~1025 cm^{-1} to the mannuronic (M) unit absorption at ~1100 cm^{-1} allows calculation of the M/G ratio that varies with particular alginate source.[13] Using this approach, alginate *A1* was determined to be ~63%G/37%M, and alginate *A2* was ~57%G/43%M. These relative proportions were supported by additional analysis: in Supplementary Figure 3b, the particular alginate lyase was a mannuronic lyase, so that the greater absorption from the digestion of *A2* than *A1* was consistent with a greater proportion of *M* in *A2*.

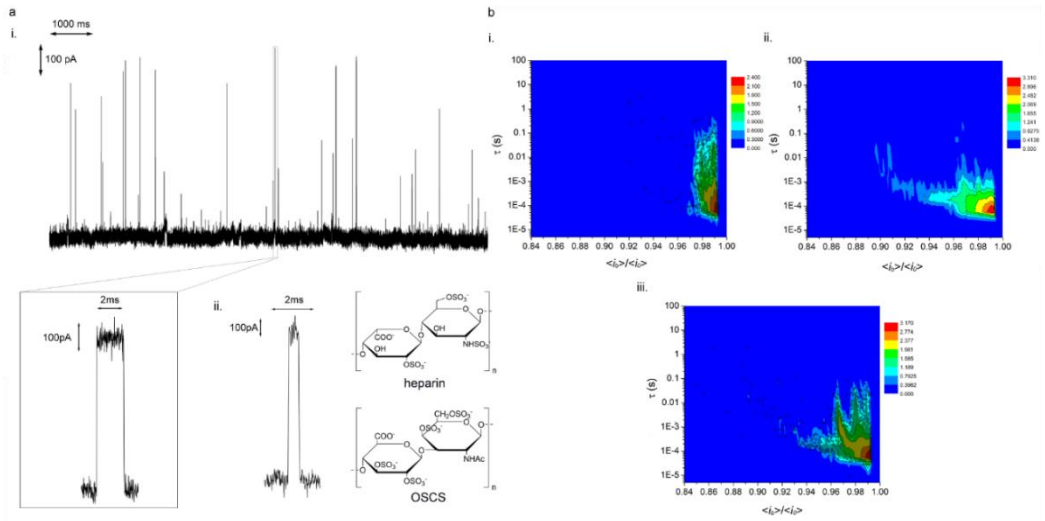

Supplementary Figure 8. Heparin and OSCS events. A representative a) i) segment of a heparin induced-current trace using a ~10 nm-diameter pore with a magnified current event from the same trace, and from ii) OSCS through the same pore in response to a -200 mV applied voltage in 4 M KCl at pH ~7. b) Contour+scatter plots of i) heparin, ii) OSCS and iii) heparin contaminated with OSCS through a ~14 nm diameter pore.

Recognition Flag Generation

Recognition flag generation was done using custom codes written in Mathematica 11.0.1.0 (Wolfram, Champaign, IL). (1) All individual events were histogrammed with respect to f_b using a bin width of 0.0025 (using nanopores with diameters from ~8-14 nm, and determined using the USP heparin data). (2) Any bin with counts below 0.5% of the maximum bin count were removed, and all counts were then normalized. (3) The OSCS identification threshold was taken to be at the nearest bin at the distance of three standard deviations (after the 0.5% filter) from the bin with the maximum number of counts. (4) When events had been detected at f_b below this threshold, the recognition flag was set to red to signal the presence of OSCS; it was otherwise left white.

(5) All individual events were then histogrammed with respect to the logarithm ($\log_{10}$) of the event duration (τ) using a bin width of 0.25 (here, determined using the USP OSCS data). (6) The same 0.5% filter was applied to these histograms, which then had their counts normalized. (7) The event duration threshold was taken to be the nearest bin at the distance of three standard deviations (after the 0.5% filter) from the bin with the maximum number of

counts. (8) When events had been detected at $\log_{10}\tau$ above this threshold, the recognition flag was set to red to signal the presence of heparin; it was otherwise left white.

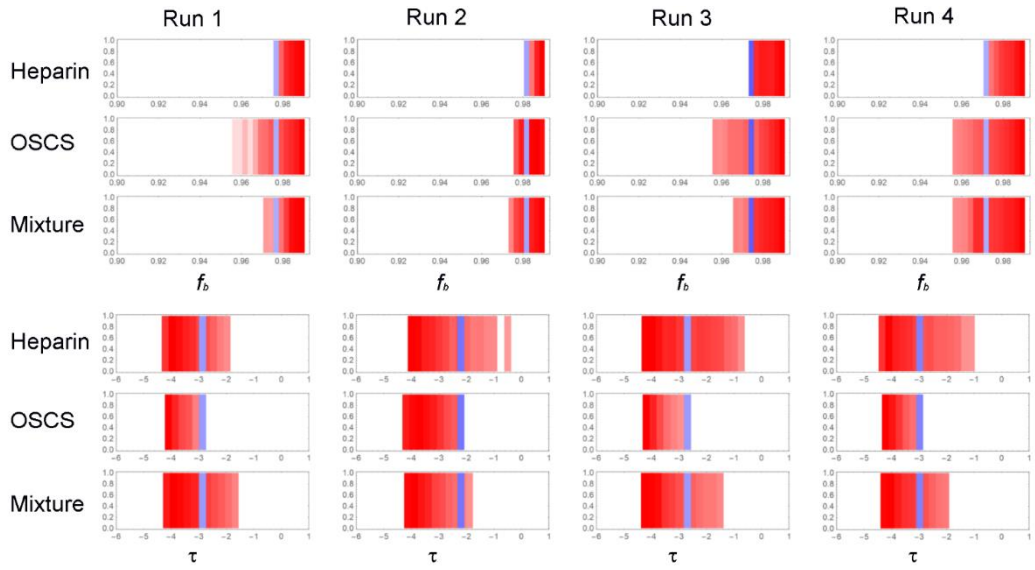

Supplementary Figure 9. Hue plots of show the outcomes of recognition flag generation (and measurement statistics—see procedure detailed above) after steps 3 (top) and 7 (bottom), based on $f_b = \langle i_b \rangle / \langle i_0 \rangle$ and $\log_{10}\tau$ of the individual events. The identification threshold, determined by the measurement statistics of each run, is given by the blue line. The corresponding final recognition flags, showing successful detection of the toxic OSCS impurity across four independent trials in ~8.6, 9.8, 9.9, and 13.6 nm (left to right), are shown in Figure 5.

---

1. Trivedi, D.M. in Electrical and Computer Engineering, Vol. Master of Applied Science 91 (The University of British Columbia, Vancouver; 2009).
2. Kwok, H., Briggs, K. & Tabard-Cossa, V. Nanopore Fabrication by Controlled Dielectric Breakdown. *PLoS ONE* **9**, e92880 (2014).
3. Frament, C.M. & Dwyer, J.R. Conductance-Based Determination of Solid-State Nanopore Size and Shape: An Exploration of Performance Limits. *J. Phys. Chem. C* **116**, 23315-23321 (2012).
4. Kowalczyk, S.W., Grosberg, A.Y., Rabin, Y. & Dekker, C. Modeling the conductance and DNA blockade of solid-state nanopores. *Nanotechnology* **22**, 315101 (2011).
5. Lee, C. et al. Large Apparent Electric Size of Solid-State Nanopores Due to Spatially Extended Surface Conduction. *Nano Lett.* **12**, 4037-4044 (2012).

6. Huggins, M.L. The Viscosity of Dilute Solutions of Long-Chain Molecules. IV. Dependence on Concentration. *J. Am. Chem. Soc.* **64**, 2716-2718 (1942).
7. Clementi, F., Mancini, M. & Moresi, M. Rheology of alginate from Azotobacter vinelandii in aqueous dispersions. *J. Food Eng.* **36**, 51-62 (1998).
8. Armstrong, J.K., Wenby, R.B., Meiselman, H.J. & Fisher, T.C. The Hydrodynamic Radii of Macromolecules and Their Effect on Red Blood Cell Aggregation. *Biophys. J.* **87**, 4259-4270 (2004).
9. Draréni, J. & Roy, S. in Image Analysis and Recognition, Edn. 1. (eds. M. Kamel & A. Campilho) 558-568 (Springer-Verlag Berlin Heidelberg, 2007).
10. Foulger, J.H. THE USE OF THE MOLISCH (α-NAPHTHOL) REACTIONS IN THE STUDY OF SUGARS IN BIOLOGICAL FLUIDS. *J. Biol. Chem* **92**, 345-353 (1931).
11. Hallal, J.L.J., Lucho, A.M.S. & Gonçalves, R.S. Electrochemical polymerization of furfural on a platinum electrode in aqueous solutions of potassium biphthalate. *Materials Research* **8**, 23-29 (2005).
12. Skidmore, M.A., Guimond, S.E., Dumax-Vorzet, A.F., Yates, E.A. & Turnbull, J.E. Disaccharide compositional analysis of heparan sulfate and heparin polysaccharides using UV or high-sensitivity fluorescence (BODIPY) detection. *Nat. Protocols* **5**, 1983-1992 (2010).
13. Pereira, L., Sousa, A., Coelho, H., Amado, A.M. & Ribeiro-Claro, P.J.A. Use of FTIR, FT-Raman and 13C-NMR spectroscopy for identification of some seaweed phycocolloids. *Biomol. Eng* **20**, 223-228 (2003).

Supplementary Information

Detection and discrimination of glycopolymers in a solid-state nanopore

Jonathan W. Nichols, Melissa Morris, Y.M. Nuwan D.Y. Bandara, Buddini Iroshika Karawdeniya, Robert B. Chevalier and Jason R. Dwyer*

Department of Chemistry, University of Rhode Island, 140 Flagg road, Kingston, 02881, USA.

*jason_dwyer@uri.edu

Reagents and Materials.

The following materials, identified by their product number and specification, were obtained from Sigma-Aldrich Corporation (St. Louis, MO, USA): Potassium chloride (60130, puriss. p.a., ≥99.5% (AT)); Sodium chloride (S7653, BioXtra, , ≥99.5% (AT)); Lithium chloride (213233, ReagentPlus ® ≥99%); HEPES potassium salt (H0527, ≥99.5% (titration)); and hydrochloric acid (320331, ACS reagent, 37%). Glycopolymers were synthesized by Blais Leeber, of the Group of Amit Basu at Brown University, according to reference[6]. Silicon-rich LPCVD silicon nitride (nominally) 10 nm-thick membranes on 200 µm-thick silicon frame (NT001Z and NT005Z; with reported membrane thicknesses for Lot # L8 10.5±0.3 nm, L15 16±2 nm, L31 14±2 nm, L68 12±2 nm) were purchased from Norcada, Inc. (Alberta, Canada).

All aqueous solutions were prepared using Type I water (~18 MΩ·cm resistivity from either a Millipore Synergy UV [Billerica, MA], or American Aqua Maxicab system [Narragansett, RI, USA]); all dilutions and washes also used this water. Stericup-VP vacuum filtration systems were used to filter electrolyte solutions after preparation, and water to prepare alginate solutions (SCVPU11RE 0.10 µm pore size in polyethersulfone membrane; EMD Millipore Corporation [MA, USA]).

Ag/AgCl electrodes were made from 1.0 mm-diameter silver wire (Alfa Aesar 11434, annealed, 99.9% (metals basis)) by soaking overnight in sodium hypochlorite (Alfa Aesar 33369, 11-15% available chlorine). Electrodes were insulated using shrink-wrap PTFE tubing (McMaster-Carr, 7960K21, high-temperature harsh environment tubing, moisture seal, heat-shrink, 0.07" ID before; and 7564K67, high-temperature harsh environment tubing, heat-shrink, 0.08" ID before, 0.05" ID after) and connected to electronics using pins (Connectivity TE Connectivity / AMP 205090-1 D sub circular connector contact, AMPLIMITE 109 Series, Socket, Crimp, 20-24 AWG). Nanopore chips were compressed between silicone gaskets (McMaster-Carr, 86435K43, high-temperature silicone rubber sheet, ultra-thin, 12" x 12", 0.015" thick, 35A durometer) in custom-machined PTFE holders with ~500 µL sample wells.[1]

Silicone tubing with ID 1.0 mm x OD 3.0 mm was obtained from Nanion Technologies GmbH, Munich, Germany.

Instrumental Details.

Measurements of solution pH and conductivity were with an Orion Star™ pH meter and Orion™ ROSS Ultra™ Refillable pH/ATC Triode™ Combination Electrodes and Orion™ DuraProbe™ 4-Electrode Conductivity Cells (Thermo Fisher Scientific Inc, MA, USA).

Nanopore formation by dielectric breakdown was performed using programmable DC power supplies (Model 9121A, B&K Precision Corporation, CA, USA) interfaced to a home-built circuit;[2] real-time current measurements were by a 428-Programmable Current Amplifier (Keithley Instruments, Cleveland, OH, USA) interfaced to NI USB 6351 DAQ card using LabView-based (National Instruments Corp., TX, USA) software to control the applied voltage.

All nanopore measurements were performed using an Axopatch 200B amplifier (Axon Instruments, Foster City, CA, USA) in voltage clamp mode. The amplifier was interfaced to a computer system using a data acquisition card (779512-01 NI PCIE-6251 M Series with 777960-01 NI BNC-2120 shielded connector block) and control software written in LabView. Current-versus-time measurements were typically acquired for 30 min (1× 30 min) at 100 kHz acquisition rates with the 4-pole low pass Bessel filter built-in to the Axopatch 200B set to 10 kHz. Measurements of nanopore conductance were acquired at a rate of 10 kHz, with the filter set to 1 kHz.

General procedure.

Nanopores in the ~10 nm-thick silicon nitride membranes were fabricated by controlled dielectric breakdown using 11-15.5 V DC applied potentials.[2] The nanopore formation was carried out in 1 M KCl electrolyte, HEPES-buffered to pH ~7, and the membranes and pores were secured in custom-machined PTFE holders with ~500 µL sample wells.

Nanopore conductances, *G*, were the slope of the fit to the experimental Ohmic current-voltage data, measured in 1 M KCl electrolyte buffered with HEPES at pH ~7. The corresponding nominal nanopore diameters were calculated using a conductance model (including bulk, surface, and access resistance terms) and cylindrical nanopore shape suitable for this salt concentration and fabrication method, $G = \left(\frac{1}{G_{\text{bulk}}+G_{\text{surface}}} + \frac{1}{G_{\text{access}}}\right)^{-1}$.[2-5] Nanopores used for measurements produced stable open-pore (analyte-free) currents at the salt concentrations used.

All electrolyte solutions were HEPES-buffered (10 mM) to pH 3-7 (adjusted with dropwise addition of concentrated hydrochloric acid), and measurements were carried out using filtered solutions with 1.0 M KCl concentrations. Solutions of 0.2% (w/v) and 0.02 % (w/v) (S)gal-(30,90) were made by dissolving the solids in filtered Type I water. For routine measurements and unless otherwise specified, 5 µL aliquots were added to the headstage side (Figure 1), leaving the ground side free of initially added analyte. Current blockages were extracted using a current-threshold analysis. Any current blockages exceeding 100 s ($\lesssim 0.1\%$ of the total number) were not included in analyses.

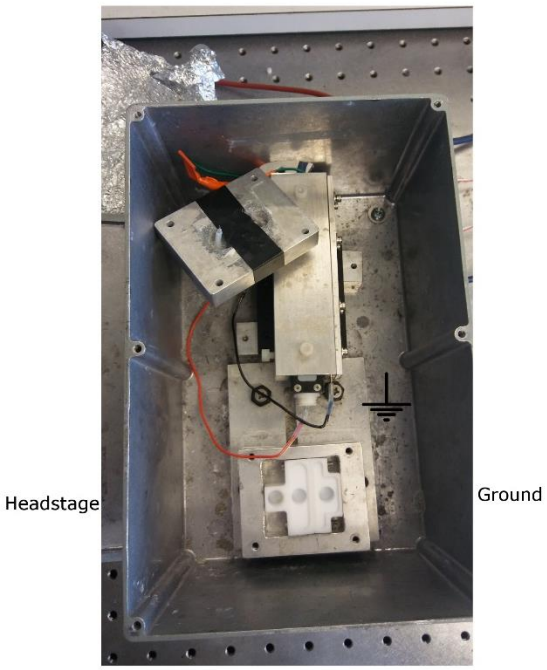

Figure 1: Set-up of nanopore measurements used on an Axopatch 200B patch clamp amplifier. The voltage is applied from the headstage side to the ground side connected by two electrodes. All measurements were done by injecting into the headstage side electrolyte well of the PTFE holder. The nanopore is sandwiched between the two wells.

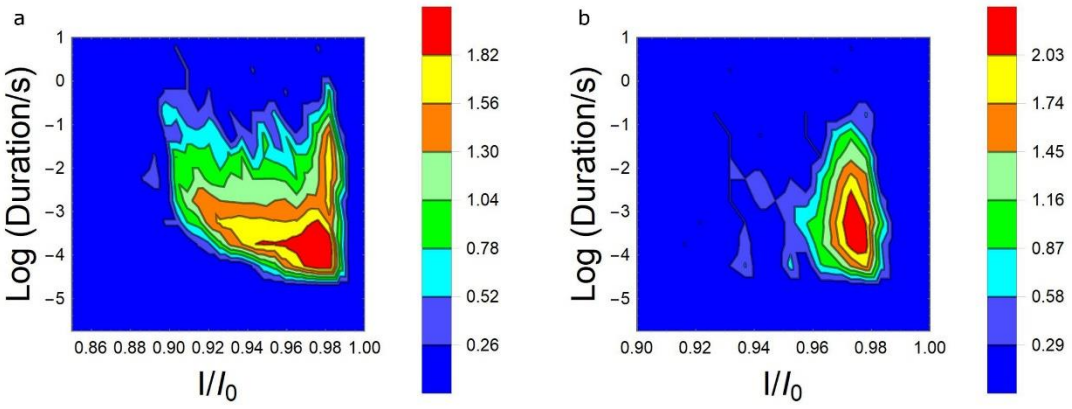

Figure 2: Event counts (log_{10} of the color axis) of 5µL of Sgal-30 and mixtures of 2.5 µL Sgal-30 and Sgal-90 in a) 1M LiCl, and b) 1M NaCl both at pH=4.3 at -200 mV applied voltage when passed through a ~7 nm nanopore for 10 minutes. Although Sgal-30 and Sgal-90 were both readily detected under these conditions, differentiation between the two was not feasible.

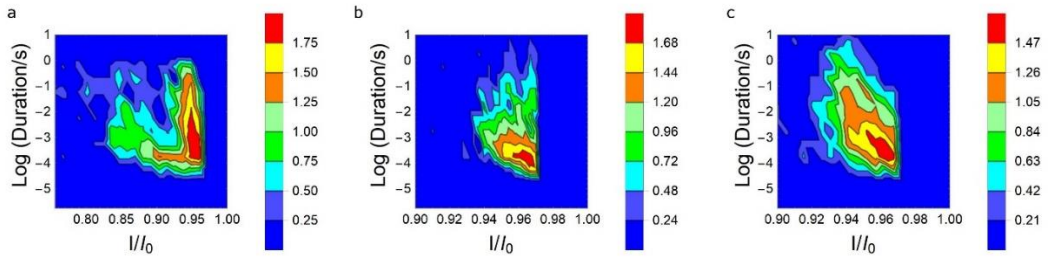

Figure 3: Event counts (log_{10} of the color axis) of 5µL of 0.02% (w/v) a) Sgal-30, b) Sgal-90, and c) 2.5µL Sgal-30 and 2.5µL Sgal-90 in a ~15 nm nanopore in 1M KCl, 10 mM HEPES, pH=3, at -50 mV applied for 30 minutes. Under these conditions there is an inability to distinguish between Sgal-30 and Sgal-90.

Salt type	1M LiCl	1M NaCl	1M KCl
# of Recorded Events	65	137	1882

Table 1: Number of recorded events in a ~17 nm nanopore after the addition of 3 µL of 0.02% (w/v) Sgal-30 with an applied voltage of -200 mV for 20 minutes. Given the much higher event frequency using KCl, it was used in all further experiments.

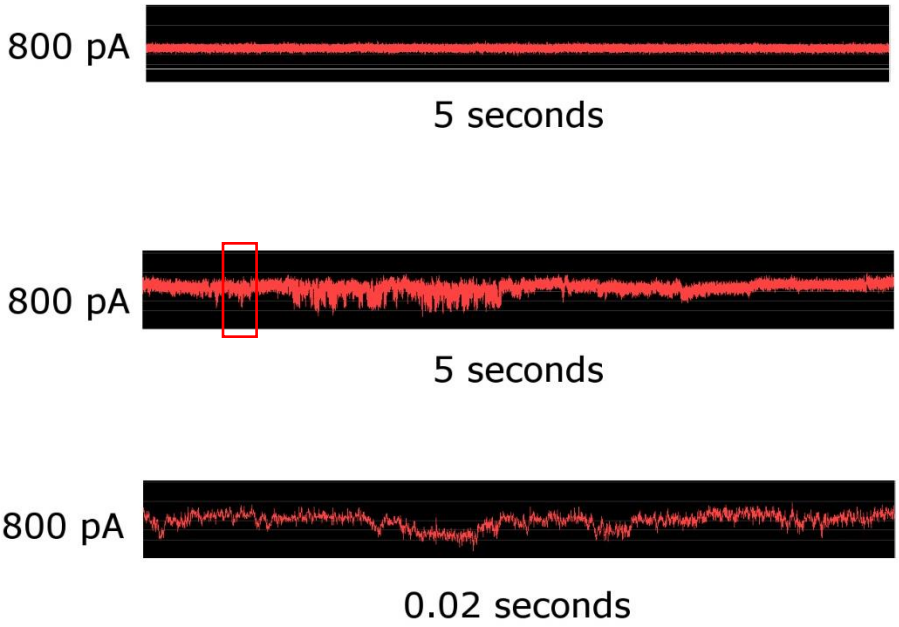

Figure 4: Current trace of a ~17 nm nanopore at -50 mV when no analyte was present in the headstage side electrolyte well of the nanopore (top) compared to that when 5 µL of 0.02% (w/v) Sgal-30 and 5 µL of 0.02% (w/v) poly-L-lysine was run at +50 mV to try and detect an Sgal-30-poly-L-lysine complex (middle). A zoomed in portion of the middle section (bottom) shows current drops but failed to provide enough signal-to-noise to distinguish the current drops as events.

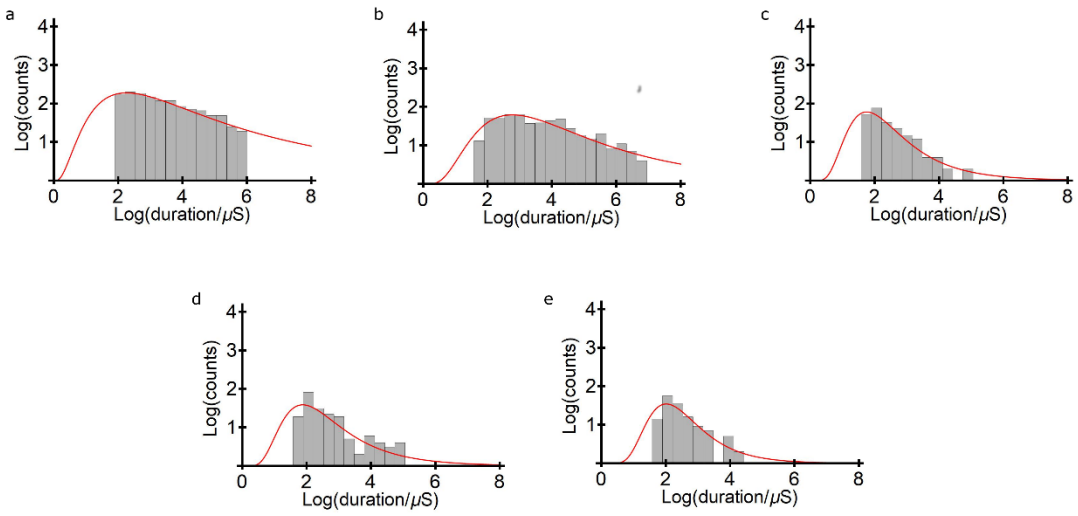

Figure 5: Histograms in duration of $\log_{10}$ of 5 µL of 0.02% Sgal-30 in 1M KCl, 10 mM HEPES, at -50 mV at a) pH=3 b) pH=4 c) pH=5 d) pH=6 and e) pH=7 in a ~15 nm nanopore

1. Trivedi, D.M. in Electrical and Computer Engineering, Vol. Master of Applied Science 91 (The University of British Columbia, Vancouver; 2009).

2. Kwok, H., Briggs, K. & Tabard-Cossa, V. Nanopore Fabrication by Controlled Dielectric Breakdown. *PLoS ONE* **9**, e92880 (2014).

3. Frament, C.M. & Dwyer, J.R. Conductance-Based Determination of Solid-State Nanopore Size and Shape: An Exploration of Performance Limits. *J. Phys. Chem. C* **116**, 23315-23321 (2012).

4. Kowalczyk, S.W., Grosberg, A.Y., Rabin, Y. & Dekker, C. Modeling the conductance and DNA blockade of solid-state nanopores. *Nanotechnology* **22**, 315101 (2011).

5. Lee, C. et al. Large Apparent Electric Size of Solid-State Nanopores Due to Spatially Extended Surface Conduction. *Nano Lett.* **12**, 4037-4044 (2012).

6. Okoth, R., Basu, A. End-labeled amino terminated monotelechelic glycopolymers generated by ROMP and Cu(I)-catalyzed azide–alkyne cycloaddition *Beilstein J. Org. Chem.* **9**, 608–612 (2013).

BIBLIOGRAPHY

Preface

1. Kwon, D. S., Gregorio, G., Bitton, N., Hendrickson, W. A. & Littman, D. R. DC-SIGN-Mediated Internalization of HIV Is Required for Trans-Enhancement of T Cell Infection. *Immunity* **16,**135–144 (2002).
2. Kooyk, Y. V. & Rabinovich, G. A. Protein-glycan interactions in the control of innate and adaptive immune responses. *Nature Immunology* **9,**593–601 (2008).
3. Puffer, E. B., Pontrello, J. K., Hollenbeck, J. J., Kink, J. A. & Kiessling, L. L. Activating B Cell Signaling with Defined Multivalent Ligands. *ACS Chemical Biology* **2,**252–262 (2007).
4. Collins, B. E. *et al.*High-Affinity Ligand Probes of CD22 Overcome the Threshold Set by cis Ligands to Allow for Binding, Endocytosis, and Killing of B Cells. *The Journal of Immunology* **177,** 2994–3003 (2006).
5. Collins, B. E. *et al.*Masking of CD22 by cis ligands does not prevent redistribution of CD22 to sites of cell contact. *Proceedings of the National Academy of Sciences* **101,** 6104–6109 (2004).
6. Rabinovich, G. A., Kooyk, Y. V. & Cobb, B. A. Glycobiology of immune responses. *Annals of the New York Academy of Sciences* **1253 ,**1–15 (2012).
7. Varki, A. Biological roles of oligosaccharides: all of the theories are correct. *Glycobiology* **3,** 97–130 (1993).
8. Dalziel, M., Crispin, M., Scanlan, C.N., Zitzmann, N. & Dwek, R.A. Emerging Principles for the Therapeutic Exploitation of Glycosylation. *Science* **334**, 75-79 (2011).
9. Ernst, B. & Magnani, J.L. From carbohydrate leads to glycomimetic drugs. *Nat Rev Drug Discov* **8**, 661-677 (2009).
10. Pinho, S.S. & Reis, C.A. Glycosylation in cancer: mechanisms and clinical implications. *Nat Rev Cancer* **15**, 540-555 (2015).
11. Szajek, A.Y., Chess, E., Johansen, K., Gratzl, G., Gray, E., Keire, D., Linhardt, R. J., Liu, J., Morris, T., Mulloy, B., Nasr, M., Shriver, Z., Torralba, P., Viskov, C., Williams, R., Woodcock, J., Workman, W., Al-Hakim, A. The US regulatory and pharmacopeia response to the global heparin contamination crisis. *Nature Biotechnology* **34**, 625–630 (2016)
12. Liu, H., Zhang, Z. & Linhardt, R.J. Lessons learned from the contamination of heparin. *Natural Product Reports* **26**, 313-321 (2009).
13. Oh, Y. I., Sheng, G. J., Chang, S.-K. & Hsieh-Wilson, L. C. Tailored Glycopolymers as Anticoagulant Heparin Mimetics. *Angewandte Chemie* **125,**12012–12015 (2013). Okoth, R., Basu, A. End-labeled amino terminated monotelechelic glycopolymers generated by ROMP and Cu(I)-catalyzed azide–alkyne cycloaddition *Beilstein J. Org. Chem.* **9**, 608–612 (2013).